
CHAPTER 1

Bloch oscillations and Wannier-Stark
localization in semiconductor
superlattices

Fausto Rossi

*Istituto Nazionale per la Fisica della Materia
Dipartimento di Fisica, Università di Modena
Via G. Campi 213/A, I-41100 Modena, Italy*

1 Introduction

Ever since the initial applications of quantum mechanics to the dynamics of electrons in solids, the analysis of Bloch electrons moving in a homogeneous electric field has been of central importance.

By employing semiclassical arguments, in 1928 Bloch [1] demonstrated that, a wave packet given by a superposition of single-band states peaked about some quasimomentum, $\hbar\mathbf{k}$, moves with a group velocity given by the gradient of the energy-band function with respect to the quasimomentum and that the rate of change of the quasimomentum is proportional to the applied field \mathbf{F} . This is often referred to as the “acceleration theorem”:

$$\hbar\dot{\mathbf{k}} = e\mathbf{F} . \quad (1)$$

Thus, in the absence of interband tunneling and scattering processes, the quasimomentum of a Bloch electron in a homogeneous and static electric field will be uniformly accelerated into the next Brillouin zone in a repeated-

zone scheme (or equivalently undergoes an Umklapp process back in to the first zone). The corresponding motion of the Bloch electron through the periodic energy-band structure, shown in Fig. 1, is called “Bloch oscillation”; It is characterized by an oscillation period $\tau_B = h/eFd$, where d denotes the lattice periodicity in the field direction.

There are two mechanisms impeding a fully periodic motion: interband tunneling and scattering processes. Interband tunneling is an intricate problem and still at the center of a continuing debate. Early calculations of the tunneling probability into other bands in which the electric field is represented by a time-independent scalar potential were made by Zener [2] using a Wentzel-Kramers-Brillouin generalization of Bloch functions, by Houston [3] using accelerated Bloch states (Houston states), and subsequently by Kane [4] and Argyres [5] who employed the crystal-momentum representation. Their calculations lead to the conclusion that the tunneling rate per Bloch period is much less than unity for electric fields up to 10^6 V/cm for typical band parameters corresponding to elemental or compound semiconductors.

Despite the apparent agreement among these calculations, the validity of employing the crystal-momentum representation or Houston functions to describe electrons moving in a non-periodic (crystal plus external field) potential has been disputed. The starting point of the controversy was the original paper by Wannier [6]. He pointed out that, due to the translational symmetry of the crystal potential, if $\phi(\mathbf{r})$ is an eigenfunction of the scalar-potential Hamiltonian (corresponding to the perfect crystal plus the external field) with eigenvalue ϵ , then any $\phi(\mathbf{r}+n\mathbf{d})$ is also an eigenfunction with eigenvalue $\epsilon + n\Delta\epsilon$, where $\Delta\epsilon = eFd$ is the so-called Wannier-Stark splitting (\mathbf{d} being the primitive lattice vector along the field direction). He concluded that the translational symmetry of the crystal gives rise to a discrete energy spectrum, the so-called Wannier-Stark ladder. The states corresponding to these equidistantly spaced levels are localized states, as schematically shown in Fig. 2 for the case of a semiconductor superlattice. The degree of this Wannier-Stark localization depends on the strength of the applied field.

The existence of such energy quantization was disputed by Zak [7], who pointed out that for the case of an infinite crystal the scalar potential $-\mathbf{F}\cdot\mathbf{r}$ is not bounded, which implies a continuous energy spectrum. Thus, the main point of the controversy was related to the existence (or absence) of Wannier-Stark ladders. More precisely, the point was to decide if interband tunneling (neglected in the original calculation by Wannier [6]) is so strong to destroy the Wannier-Stark energy quantization (and the corresponding Bloch oscillations) or not. We will give a brief historical account of this long-standing controversy in the following section.

It is only during the last decade that this controversy came to an end. From a theoretical point of view, most of the formal problems related to

the non-periodic nature of the scalar potential (superimposed to the periodic crystal potential) were finally removed by using a vector-potential representation of the applied field [8, 9]. Within such vector-potential picture, upper boundaries for the interband tunneling probability have been established at a rigorous level, which show that an electron may execute a number of Bloch oscillations before tunneling out of the band [9, 10, 11], in qualitatively good agreement with the earlier predictions of Zener and Kane [2, 4].

The second mechanism impeding a fully periodic motion is scattering by phonons, impurities, etc. (see Fig. 1). This results in lifetimes shorter than the Bloch period τ_B for all reasonable values of the electric field, so that Bloch oscillations should not be observable in conventional solids.

In superlattices, however, the situation is much more favourable because of the smaller Bloch period τ_B resulting from the small width of the mini-Brillouin zone in the field direction [12].

Indeed, the existence of Wannier-Stark ladders as well as Bloch oscillations in superlattices has been confirmed by a number of recent experiments [13]. The photoluminescence and photocurrent measurements of the biased GaAs/GaAlAs superlattices performed by Mendez and coworkers [14], together with the electroluminescence experiments by Voisin and coworkers [15], provided the earliest experimental evidence of the field-induced Wannier-Stark ladders in superlattices. A few years later, Feldmann and coworkers [16] were able to measure Bloch oscillations in the time domain through a four-wave-mixing experiment originally suggested by von Plessen and Thomas [17]. A detailed analysis of the Bloch oscillations in the four-wave-mixing signal (which reflects the interband dynamics) has been also performed by Leo and coworkers [18, 19].

In addition to the above interband-polarization analysis, Bloch oscillations have been also detected by monitoring the intraband polarization which, in turn, is reflected by anisotropic changes in the refractive index [13]. Measurements based on transmittive electrooptic sampling (TEOS) have been performed by Dekorsy and coworkers [20, 21]. Finally Bloch oscillations were recently measured through a direct detection of the Terahertz (THz) radiation in semiconductor superlattices [22, 23].

The aim of this chapter is to present a general approach to the study of the ultrafast carrier dynamics in semiconductor superlattices. Our theoretical description, based on the density matrix formalism discussed in chapter 6, is presented in Sect. 3. It allows to derive a set of kinetic equations which accounts for interband tunneling as well as scattering processes and it is valid in any quantum-mechanical representation.

In Sect. 4 the freedom of choice of the basis states in our kinetic formulation will be used to introduce the two typical pictures commonly used for the description of semiconductor superlattices, namely, the Bloch-oscillation and Wannier-Stark pictures. In particular, we will see that they

correspond to the two equivalent vector- and scalar-potential representations of the applied field. This will implicitly state the total equivalence of the Bloch-oscillation and Wannier-Stark representations, which in turn shows that the so-called “semiclassical Bloch picture” is on the contrary a rigorous quantum-mechanical result.

Finally, in Sect. 5 we will review and discuss some simulated experiments.

2 Hystorical background

In this section we give a brief historical account concerning the controversy on the existence of Wannier-Stark ladders mentioned above. Some of the main criticisms to the pioneering works on Bloch oscillations may be summarized as follows.

- (i) The eigenvalues of the time-independent Schrödinger equation are not quantized but they form a continuous spectrum.
- (ii) Since the Hamiltonian within the scalar-potential representation is not periodic, it is not clear whether one can employ the periodic Bloch states or Houston functions: a superposition of Bloch functions will automatically yield a periodic function while the solution of the time-dependent Schrödinger equation is, in general, not periodic.
- (iii) The position operator (entering the scalar potential) is ill-defined within the crystal-momentum representation.

In a series of papers, Wannier [6, 24] and coworkers [25, 26] have argued that in the presence of a homogeneous electric field, one can modify the Bloch states in such a way that there is no interband coupling and an electron in a crystal will move within one band with its \mathbf{k} changing in time according to the acceleration theorem in Eq. (1). Furthermore, if $\mathbf{k}(t=0)$ is in the direction of a reciprocal-lattice vector, the periodic motion in \mathbf{k} -space gives rise to an energy quantization with $\Delta\epsilon = eFd$ ($d = \frac{2\pi}{G}$ being the lattice constant along the field direction), the so-called Wannier-Stark ladders. “The basis for this idea is that energy bands arise from the translational symmetry of the crystalline field and this symmetry is not removed physically by the presence of the applied field” [24], i.e. the field is still periodic with the lattice period.

These arguments have been refuted by Zak [7], who shows that, although it immediately follows from the one-dimensional time-independent Schrödinger equation for an infinite crystal with lattice constant d , that if ϵ is an eigenvalue, $\epsilon + n\Delta\epsilon$ is also an eigenvalue, the spectrum of ϵ is continuous with $-\infty < \epsilon < +\infty$, so the Wannier-Stark ladders do not exist.

Wannier [27] has argued that Zak’s criticisms of his proof are not valid, but concedes that the Stark ladders may be metastable resonant states limited by interband tunneling, as for the case of the hydrogen atom in

the presence of a static field. However, Wannier's arguments were immediately rejected by Zak [28], who claims that Wannier's original equation was incorrect.

A few years later, Rabinovitch and Zak [29] have extended Zak's [7] earlier arguments to the question of Bloch oscillations. They argue that since neglecting the interband coupling terms in the time-independent Schrödinger equation leads incorrectly to energy quantization, then the interband terms cannot be neglected in the lowest approximation because they are the same order as the terms retained. By applying the same reasoning to the time-dependent equation, they conclude (without offering a proof) that neglecting the interband terms as a first approximation, as done by Houston [3], is incorrect for times equal to or longer than the Bloch-oscillation period τ_B . From their conclusions it follows that the typical diagrams which are commonly used to portray trajectories of $\mathbf{k}(t)$ superimposed upon the energy-band structure (see Fig. 1) are incorrect and misleading.

Nevertheless, shortly before these latter arguments appeared, experimental results were obtained by Koss and Lambert [30], which were interpreted as supporting the existence of Wannier-Stark levels. They found that the observed low-temperature optical absorption of GaAs in a strong electric field ($F = 10^5 \text{V/cm}$) closely followed the theoretical predictions of Callaway [31], which, in turn, were based on employing Kane's wavefunctions and Wannier-Stark quantized energy levels.

3 Theoretical analysis

In this section we will try to review and discuss in a systematic way the basic ideas used in the theoretical analysis of semiconductor superlattices. As already pointed out in Sect. 1, the phenomena under investigation, i.e. Bloch oscillations and Wannier-Stark localization, are peculiar of any lattice structure. Therefore, even if most of the results discussed in this chapter refer to semiconductor superlattices, the general formulation presented in this section applies to any crystalline structure.

3.1 Physical system

In order to study the optical and transport properties of semiconductor superlattices, let us consider a gas of carriers in a crystal under the action of an applied electromagnetic field. The carriers will experience their mutual interaction as well as the interaction with the phonon modes of the crystal. Such physical system can be described by the following Hamiltonian:

$$\mathbf{H} = \mathbf{H}_c + \mathbf{H}_p + \mathbf{H}_{cc} + \mathbf{H}_{cp} + \mathbf{H}_{pp} . \quad (2)$$

The first term describes the noninteracting-carrier system in the presence of the external electromagnetic field while the second one refers to

the free-phonon system. The last three terms describe many-body contributions: they refer, respectively, to carrier-carrier, carrier-phonon, and phonon-phonon interactions.

In order to discuss their explicit form, let us introduce the usual second-quantization field operators $\Psi^\dagger(\mathbf{r})$ and $\Psi(\mathbf{r})$. They describe, respectively, the creation and the annihilation of a carrier in \mathbf{r} . In terms of the above field operators the carrier Hamiltonian \mathbf{H}_c can be written as

$$\mathbf{H}_c = \int d\mathbf{r} \Psi^\dagger(\mathbf{r}) \left[\frac{(-i\hbar\nabla_{\mathbf{r}} - \frac{e}{c}\mathbf{A}(\mathbf{r}, t))^2}{2m_o} + e\varphi(\mathbf{r}, t) + V^l(\mathbf{r}) \right] \Psi(\mathbf{r}) . \quad (3)$$

Here, $V^l(\mathbf{r})$ denotes the periodic potential due to the perfect crystal while $\mathbf{A}(\mathbf{r}, t)$ and $\varphi(\mathbf{r}, t)$ denote, respectively, the vector and scalar potentials corresponding to the external electromagnetic field. Since we are interested in the electrooptical properties as well as in the ultrafast dynamics of photoexcited carriers, the electromagnetic field acting on the crystal—and the corresponding electromagnetic potentials—will be the sum of two different contributions: the high-frequency laser field responsible for the ultrafast optical excitation and the additional electromagnetic field acting on the photoexcited carriers on a longer time-scale. More specifically, by denoting with the labels 1 and 2 these two contributions, we can write

$$\mathbf{A}(\mathbf{r}, t) = \mathbf{A}_1(\mathbf{r}, t) + \mathbf{A}_2(\mathbf{r}, t) , \quad \varphi(\mathbf{r}, t) = \varphi_1(\mathbf{r}, t) + \varphi_2(\mathbf{r}, t) \quad (4)$$

and recalling that

$$\mathbf{E}(\mathbf{r}, t) = -\frac{1}{c} \frac{\partial}{\partial t} \mathbf{A}(\mathbf{r}, t) - \nabla_{\mathbf{r}} \varphi(\mathbf{r}, t) , \quad \mathbf{B}(\mathbf{r}, t) = \nabla_{\mathbf{r}} \times \mathbf{A}(\mathbf{r}, t) \quad (5)$$

we have

$$\mathbf{E}(\mathbf{r}, t) = \mathbf{E}_1(\mathbf{r}, t) + \mathbf{E}_2(\mathbf{r}, t) , \quad \mathbf{B}(\mathbf{r}, t) = \mathbf{B}_1(\mathbf{r}, t) + \mathbf{B}_2(\mathbf{r}, t) . \quad (6)$$

Equation (5), which gives the electromagnetic fields in terms of the corresponding vector and scalar potentials, reflects the well known gauge freedom: there is an infinite number of possible combinations of \mathbf{A} and φ which give rise to the same electromagnetic field $\{\mathbf{E}, \mathbf{B}\}$. We will use such freedom of choice for the laser field (term 1): we assume a homogeneous (space-independent) laser field $\mathbf{E}_1(t)$ fully described by the scalar potential

$$\varphi_1(\mathbf{r}, t) = -\mathbf{E}_1(t) \cdot \mathbf{r} . \quad (7)$$

This assumption, which corresponds to the well known dipole approximation, is well justified as long as the space-scale of interest is small compared to the light wavelength. The explicit form of the laser field considered in this chapter is

$$E_1(t) = E^+(t) + E^-(t) = E_o(t)e^{i\omega_L t} + E_o^*(t)e^{-i\omega_L t} , \quad (8)$$

where $E_o(t)$ is the amplitude of the light field and ω_L denotes its central frequency.

With this particular choice of the electromagnetic potentials describing the laser field, the Hamiltonian in Eq. (3) can be rewritten as

$$\mathbf{H}_c = \mathbf{H}_c^o + \mathbf{H}_{cl} , \quad (9)$$

where

$$\mathbf{H}_c^o = \int d\mathbf{r} \Psi^\dagger(\mathbf{r}) \left[\frac{(-i\hbar\nabla_{\mathbf{r}} - \frac{e}{c}\mathbf{A}_2(\mathbf{r}, t))^2}{2m_o} + e\varphi_2(\mathbf{r}, t) + V^l(\mathbf{r}) \right] \Psi(\mathbf{r}) \quad (10)$$

describes the carrier system in the crystal under the action of the electromagnetic field 2 only, while

$$\mathbf{H}_{cl} = e \int d\mathbf{r} \Psi^\dagger(\mathbf{r}) \varphi_1(\mathbf{r}, t) \Psi(\mathbf{r}) \quad (11)$$

describes the carrier-light (cl) interaction due to the laser photoexcitation.

In analogy with the carrier system, by denoting with $b_{\mathbf{q},\lambda}^\dagger$ and $b_{\mathbf{q},\lambda}$ the creation and annihilation operators for a phonon of mode λ and wavevector \mathbf{q} , the free-phonon Hamiltonian takes the form

$$\mathbf{H}_p = \sum_{\mathbf{q}\lambda} \hbar\omega_{\mathbf{q}\lambda} b_{\mathbf{q}\lambda}^\dagger b_{\mathbf{q}\lambda} , \quad (12)$$

where $\omega_{\mathbf{q}\lambda}$ is the dispersion relation for the phonon mode λ .

Let us now discuss the explicit form of the many-body contributions. The carrier-carrier interaction is described by the two-body Hamiltonian

$$\mathbf{H}_{cc} = \frac{1}{2} \int d\mathbf{r} \int d\mathbf{r}' \Psi^\dagger(\mathbf{r}) \Psi^\dagger(\mathbf{r}') V_{cc}(\mathbf{r} - \mathbf{r}') \Psi(\mathbf{r}') \Psi(\mathbf{r}) , \quad (13)$$

where V_{cc} denotes the Coulomb potential.

Let us now introduce the carrier-phonon interaction Hamiltonian

$$\mathbf{H}_{cp} = \int d\mathbf{r} \Psi^\dagger(\mathbf{r}) V_{cp}(\mathbf{r}) \Psi(\mathbf{r}) , \quad (14)$$

where

$$V_{cp} = \sum_{\mathbf{q}\lambda} \left[\tilde{g}_{\mathbf{q}\lambda} b_{\mathbf{q}\lambda} e^{i\mathbf{q}\cdot\mathbf{r}} + \tilde{g}_{\mathbf{q}\lambda}^* b_{\mathbf{q}\lambda}^\dagger e^{-i\mathbf{q}\cdot\mathbf{r}} \right] \quad (15)$$

is the electrostatic phonon potential induced by the lattice vibrations. Here, the explicit form of the coupling function $\tilde{g}_{\mathbf{q}\lambda}$ depends on the particular phonon mode λ (acoustical, optical, etc.) as well as on the coupling mechanism considered (deformation potential, polar coupling, etc.).

Let us finally discuss the phonon-phonon contribution \mathbf{H}_{pp} . The free-phonon Hamiltonian \mathbf{H}_p introduced in Eq. 12, which describes a system of noninteracting phonons, by definition accounts only for the harmonic part of the lattice potential. However, non-harmonic contributions of the

interatomic potential can play an important role in determining the lattice dynamics in highly excited systems [32], since they are responsible for the decay of optical phonons into phonons of lower frequency. In our second-quantization picture, these non-harmonic contributions can be described in terms of a phonon-phonon interaction which induces, in general, transitions between free-phonon states. Here, we will not discuss the explicit form of the phonon-phonon Hamiltonian \mathbf{H}_{pp} responsible for such a decay. We will simply assume that such phonon-phonon interaction is so efficient to maintain the phonon system in thermal equilibrium. This corresponds to neglect hot-phonon effects [33].

It is well known that the coordinate representation used so far is not the most appropriate one in describing the electron dynamics within a periodic crystal. On the contrary, it is in general more convenient to employ the representation given by the eigenstates of the noninteracting-carrier Hamiltonian —or a part of it— since it automatically accounts for some of the symmetries of the system. For the moment we will simply consider an orthonormal basis set $\{\phi_n(\mathbf{r})\}$ without specifying which part of the Hamiltonian is diagonal in such representation. This will allow us to write down equations valid in any quantum-mechanical representation. Since the noninteracting-carrier Hamiltonian is, in general, a function of time, also the basis functions ϕ_n may be time-dependent. Here, the label n denotes, in general, a set of discrete and/or continuous quantum numbers. In the absence of electromagnetic field, the above wavefunctions will correspond to the well known Bloch states of the crystal and the index n will reduce to the wavevector \mathbf{k} plus the band index ν . In the presence of a homogeneous magnetic field the eigenfunctions ϕ_n may instead correspond to Landau states. Finally, for the case of a constant and homogeneous electric field, there exist two equivalent representations: the accelerated Bloch states and the Wannier-Stark picture. Such equivalence results to be of crucial importance in understanding the relationship between Bloch oscillations and Wannier-Stark localization and, for this reason, it will be discussed in more detail in Sect. 4.

Let us now reconsider the system Hamiltonian introduced so far in terms of such ϕ_n representation. As a starting point, we may expand the second-quantization field operators in terms of the new wavefunctions:

$$\Psi(\mathbf{r}) = \sum_n \phi_n(\mathbf{r})a_n, \quad \Psi^\dagger(\mathbf{r}) = \sum_n \phi_n^*(\mathbf{r})a_n^\dagger. \quad (16)$$

The above expansion defines the new set of second-quantization operators a_n^\dagger and a_n ; They describe, respectively, the creation and annihilation of a carrier in state n .

For the case of a semiconductor crystal (which will be the only one considered in this chapter), the energy spectrum of the noninteracting-carrier Hamiltonian in Eq. (10) —or a part of it— is always characterized

by two well-separated energy regions: the valence and the conduction band. Also in the presence of an applied electromagnetic field, the periodic lattice potential V^l gives rise to a large energy gap. Therefore, we deal with two energetically well-separated regions, which suggests the introduction of the so-called electron-hole picture. This corresponds to a separation of the set of states $\{\phi_n\}$ into conduction states $\{\phi_i^e\}$ and valence states $\{\phi_j^h\}$. Thus, also the creation (annihilation) operators a_n^\dagger (a_n) introduced in Eq. (16) will be divided into creation (annihilation) electron and hole operators: c_i^\dagger (c_i) and d_j^\dagger (d_j). In terms of the new electron-hole picture, the expansion in Eq. (16) is given by:

$$\begin{aligned}\Psi(\mathbf{r}) &= \sum_i \phi_i^e(\mathbf{r})c_i + \sum_j \phi_j^{h*}(\mathbf{r})d_j^\dagger \\ \Psi^\dagger(\mathbf{r}) &= \sum_i \phi_i^{e*}(\mathbf{r})c_i^\dagger + \sum_j \phi_j^h(\mathbf{r})d_j .\end{aligned}\quad (17)$$

If we now insert the above expansion into Eq. (10), the noninteracting-carrier Hamiltonian takes the form

$$\mathbf{H}_c^\circ = \sum_{ii'} \epsilon_{ii'}^e c_i^\dagger c_{i'} + \sum_{jj'} \epsilon_{jj'}^h d_j^\dagger d_{j'} = \mathbf{H}_e^\circ + \mathbf{H}_h^\circ , \quad (18)$$

where

$$\epsilon_{ii'}^{e/h} = \pm \int d\mathbf{r} \phi_i^{e/h*}(\mathbf{r}) \left[\frac{(-i\hbar\nabla_{\mathbf{r}} - \frac{e}{c}\mathbf{A}_2)^2}{2m_o} + e\varphi_2 + V^l - \epsilon_o \right] \phi_{i'}^{e/h}(\mathbf{r}) \quad (19)$$

are just the matrix elements of the Hamiltonian in the ϕ -representation. The \pm sign refers, respectively, to electrons and holes while ϵ_o denotes the conduction-band edge. Here, we neglect any valence-to-conduction band coupling due to the external electromagnetic field and vice versa. This is well fulfilled for the systems and field-regimes we are going to discuss in this chapter. As already pointed out, the above Hamiltonian may be time-dependent. We will discuss this aspect in the following section, where we will derive our set of kinetic equations.

Let us now write in terms of our electron-hole representation the carrier-light interaction Hamiltonian introduced in Eq. (11):

$$\mathbf{H}_{cl} = - \sum_{i,j} \left[\mu_{ij}^{eh} E^-(t) c_i^\dagger d_j^\dagger + \mu_{ij}^{eh*} E^+(t) d_j c_i \right] . \quad (20)$$

The above expression has been obtained within the well known rotating-wave approximation by neglecting intraband transitions, absent for the case of optical excitations. Here, μ_{ij}^{eh} denotes the optical dipole matrix element between states ϕ_i^e and ϕ_j^h .

Similarly, the carrier-carrier Hamiltonian (13) can be rewritten as:

$$\begin{aligned}
\mathbf{H}_{cc} = & \frac{1}{2} \sum_{i_1 i_2 i_3 i_4} V_{i_1 i_2 i_3 i_4}^{cc} c_{i_1}^\dagger c_{i_2}^\dagger c_{i_3} c_{i_4} \\
& + \frac{1}{2} \sum_{j_1 j_2 j_3 j_4} V_{j_1 j_2 j_3 j_4}^{cc} d_{j_1}^\dagger d_{j_2}^\dagger d_{j_3} d_{j_4} \\
& - \sum_{i_1 i_2 j_1 j_2} V_{i_1 j_1 j_2 i_2}^{cc} c_{i_1}^\dagger d_{j_1}^\dagger d_{j_2} c_{i_2}, \tag{21}
\end{aligned}$$

where

$$V_{l_1 l_2 l_3 l_4}^{cc} = \int d\mathbf{r} \int d\mathbf{r}' \phi_{l_1}^*(\mathbf{r}) \phi_{l_2}^*(\mathbf{r}') V^{cc}(\mathbf{r} - \mathbf{r}') \phi_{l_3}(\mathbf{r}') \phi_{l_4}(\mathbf{r}) \tag{22}$$

are the Coulomb matrix elements within our ϕ -representation. The first two terms describe the repulsive electron-electron and hole-hole interaction while the last one describes the attractive electron-hole interaction. Here, we neglect terms that do not conserve the number of electron-hole pairs, i.e. impact-ionization and Auger-recombination processes [34], as well as the interband exchange interaction. This monopole-monopole approximation is justified as long as the exciton binding energy (which in semiconductors is less than 20meV) is small compared to the energy gap (which is more than 1eV).

Finally, let us rewrite the carrier-phonon interaction Hamiltonian introduced in Eq. (14):

$$\begin{aligned}
\mathbf{H}_{cp} = & \sum_{ii', \mathbf{q}\lambda} \left[g_{ii', \mathbf{q}\lambda}^e c_i^\dagger b_{\mathbf{q}\lambda} c_{i'} + g_{ii', \mathbf{q}\lambda}^{e*} c_i^\dagger b_{\mathbf{q}\lambda}^\dagger c_{i'} \right] \\
& - \sum_{jj', \mathbf{q}\lambda} \left[g_{jj', \mathbf{q}\lambda}^h d_j^\dagger b_{\mathbf{q}\lambda} d_{j'} + g_{jj', \mathbf{q}\lambda}^{h*} d_j^\dagger b_{\mathbf{q}\lambda}^\dagger d_{j'} \right] \tag{23}
\end{aligned}$$

with

$$g_{ll', \mathbf{q}\lambda}^{e/h} = \tilde{g}_{\mathbf{q}\lambda} \int d\mathbf{r} \phi_l^{e/h*}(\mathbf{r}) e^{i\mathbf{q}\cdot\mathbf{r}} \phi_{l'}^{e/h}(\mathbf{r}). \tag{24}$$

In Eq. (23) we can clearly recognize four different contributions corresponding to electron and hole phonon absorption and emission.

3.2 Kinetic description

Our kinetic description of the ultrafast carrier dynamics in semiconductor superlattices, presented in this section, is based on the density-matrix formalism. Since this approach has been already reviewed and discussed in chapter 6, here we will simply recall in our notation the kinetic equations relevant for the analysis of carrier dynamics in superlattices, generalizing the approach of chapter 6 to the case of a time-dependent quantum-mechanical representation.

The set of kinetic variables is the same considered in chapter 6. Given our electron-hole representation $\{\phi_i^e\}, \{\phi_j^h\}$, we will consider the intraband electron and hole single-particle density matrices

$$f_{ii'}^e = \langle c_i^\dagger c_{i'} \rangle, \quad f_{jj'}^h = \langle d_j^\dagger d_{j'} \rangle \quad (25)$$

as well as the corresponding interband density matrix

$$p_{ji} = \langle d_j c_i \rangle. \quad (26)$$

Here, the diagonal elements f_{ii}^e and f_{jj}^h correspond to the electron and hole distribution functions of the Boltzmann theory while the non-diagonal terms describe intraband polarizations. On the contrary, the interband density-matrix elements p_{ji} describe interband (or optical) polarizations.

In order to derive the set of kinetic equations, i.e. the equations of motion for the above kinetic variables, the standard procedure starts by deriving the equations of motion for the electron and hole operators introduced in Eq. (17):

$$c_i = \int d\mathbf{r} \phi_i^{e*}(\mathbf{r}) \Psi(\mathbf{r}), \quad d_j = \int d\mathbf{r} \phi_j^{h*}(\mathbf{r}) \Psi^\dagger(\mathbf{r}). \quad (27)$$

By applying the Heisenberg equation of motion for the field operator Ψ , i.e.

$$\frac{d}{dt} \Psi = \frac{1}{i\hbar} [\Psi, \mathbf{H}], \quad (28)$$

it is easy to obtain the following equations of motion:

$$\begin{aligned} \frac{d}{dt} c_i &= \frac{1}{i\hbar} [c_i, \mathbf{H}] + \frac{1}{i\hbar} \sum_{i'} Z_{ii'}^e c_{i'} \\ \frac{d}{dt} d_j &= \frac{1}{i\hbar} [d_j, \mathbf{H}] + \frac{1}{i\hbar} \sum_{j'} Z_{jj'}^h d_{j'} \end{aligned} \quad (29)$$

with

$$Z_{ll'}^{e/h} = i\hbar \int d\mathbf{r} \left(\frac{d}{dt} \phi_l^{e/h*}(\mathbf{r}) \right) \phi_{l'}^{e/h}(\mathbf{r}). \quad (30)$$

As for the case of Eq. (18), here we neglect again valence-to-conduction band coupling and vice versa. Compared to the more conventional Heisenberg equations of motion, the above equations contain an extra-term, the last one. It accounts for the possible time dependence of our ϕ -representation which will induce transitions between different states according to the matrix elements $Z_{ll'}$.

By combining the above equations of motion with the definitions of the kinetic variables in Eqs. (25-26), our set of kinetic equations can be

schematically written as:

$$\begin{aligned}
\frac{d}{dt} f_{i_1 i_2}^e &= \frac{d}{dt} f_{i_1 i_2}^e \Big|_{\mathbf{H}} + \frac{d}{dt} f_{i_1 i_2}^e \Big|_{\phi} \\
\frac{d}{dt} f_{j_1 j_2}^h &= \frac{d}{dt} f_{j_1 j_2}^h \Big|_{\mathbf{H}} + \frac{d}{dt} f_{j_1 j_2}^h \Big|_{\phi} \\
\frac{d}{dt} p_{j_1 i_1} &= \frac{d}{dt} p_{j_1 i_1} \Big|_{\mathbf{H}} + \frac{d}{dt} p_{j_1 i_1} \Big|_{\phi} .
\end{aligned} \tag{31}$$

They exhibit the same structure of the equations of motion (29) for the electron and hole creation and annihilation operators: a first term induced by the system Hamiltonian \mathbf{H} (which does not account for the time variation of the basis states) and a second one induced by the time dependence of the basis functions ϕ .

Let us start discussing this second term, whose explicit form is given by:

$$\begin{aligned}
\frac{d}{dt} f_{i_1 i_2}^e \Big|_{\phi} &= \frac{1}{i\hbar} \sum_{i_3 i_4} [Z_{i_2 i_4}^e \delta_{i_1 i_3} - Z_{i_3 i_1}^e \delta_{i_2 i_4}] f_{i_3 i_4}^e \\
\frac{d}{dt} f_{j_1 j_2}^h \Big|_{\phi} &= \frac{1}{i\hbar} \sum_{j_3 j_4} [Z_{j_2 j_4}^h \delta_{j_1 j_3} - Z_{j_3 j_1}^h \delta_{j_2 j_4}] f_{j_3 j_4}^h \\
\frac{d}{dt} p_{j_1 i_1} \Big|_{\phi} &= \frac{1}{i\hbar} \sum_{i_2 j_2} [Z_{j_1 j_2}^h \delta_{i_1 i_2} + Z_{i_1 i_2}^e \delta_{j_1 j_2}] p_{j_2 i_2} .
\end{aligned} \tag{32}$$

Such terms were not considered in chapter 6, where a time-independent representation has been used. As we will see in Sect. 4, they will play a central role for the description of Bloch oscillations within the vector-potential representation.

Let us now come to the first term. This, in turn, is the sum of different contributions, corresponding to the various parts of the Hamiltonian. In particular, the total Hamiltonian can be regarded as the sum of two terms, a single-particle contribution plus a many-body one:

$$\mathbf{H} = \mathbf{H}_{sp} + \mathbf{H}_{mb} = (\mathbf{H}_c^o + \mathbf{H}_{cl} + \mathbf{H}_p) + (\mathbf{H}_{cc} + \mathbf{H}_{cp} + \mathbf{H}_{pp}) . \tag{33}$$

The explicit form of the time evolution due to the single-particle Hamiltonian \mathbf{H}_{sp} (non-interacting carriers plus carrier-light interaction plus free phonons) is given by:

$$\frac{d}{dt} f_{i_1 i_2}^e \Big|_{sp} = \frac{1}{i\hbar} \left\{ \sum_{i_3 i_4} [\epsilon_{i_2 i_4}^e \delta_{i_1 i_3} - \epsilon_{i_3 i_1}^e \delta_{i_2 i_4}] f_{i_3 i_4}^e \right.$$

$$\begin{aligned}
& + \sum_{j_1} [U_{i_2 j_1} p_{j_1 i_1}^* - U_{i_1 j_1}^* p_{j_1 i_2}] \Big\} \\
\left. \frac{d}{dt} f_{j_1 j_2}^h \right|_{sp} &= \frac{1}{i\hbar} \left\{ \sum_{j_3 j_4} [\epsilon_{j_2 j_4}^h \delta_{j_1 j_3} - \epsilon_{j_3 j_1}^h \delta_{j_2 j_4}] f_{j_3 j_4}^h \right. \\
& \left. + \sum_{i_1} [U_{i_1 j_2} p_{j_1 i_1}^* - U_{i_1 j_1}^* p_{j_2 i_1}] \right\} \\
\left. \frac{d}{dt} p_{j_1 i_1} \right|_{sp} &= \frac{1}{i\hbar} \left\{ \sum_{i_2 j_2} [\epsilon_{j_1 j_2}^h \delta_{i_1 i_2} + \epsilon_{i_1 i_2}^e \delta_{j_1 j_2}] p_{j_2 i_2} \right. \\
& \left. + \sum_{i_2 j_2} U_{i_2 j_2} [\delta_{i_1 i_2} \delta_{j_1 j_2} - f_{i_2 i_1}^e \delta_{j_1 j_2} - f_{j_2 j_1}^h \delta_{i_1 i_2}] \right\} \quad (34)
\end{aligned}$$

with $U_{i_1 j_1} = -\mu_{i_1 j_1}^{e/h} E^-(t)$.

This is a closed set of equations, which is a consequence of the single-particle nature of \mathbf{H}_{sp} . In addition, we stress that the structure of the two contributions entering Eq. (31) is very similar: one can include the contribution (32) into Eq. (34) by replacing ϵ with $\epsilon + Z$.

Let us finally discuss the contributions due to the many-body part of the Hamiltonian: carrier-carrier and carrier-phonon interactions (the phonon-phonon one is not explicitly considered here). As discussed in chapter 6, for both interaction mechanisms one can derive a hierarchy of equations involving higher-order density matrices and, in order to close such equations with respect to our set of kinetic variables, approximations are needed. The lowest-order contributions to our equations of motion are given by first-order terms in the many-body Hamiltonian: Hartree-Fock level. Since we will neglect coherent-phonon states, the only Hartree-Fock contributions will come from carrier-carrier interaction. They simply result in a renormalization

$$\Delta \epsilon_{l_1 l_2}^{e/h} = - \sum_{l_3 l_4} V_{l_1 l_3 l_2 l_4}^{cc} f_{l_3 l_4}^{e/h} \quad (35)$$

of the single-particle energy matrices $\epsilon^{e/h}$ as well as in a renormalization

$$\Delta U_{i_1 j_1} = - \sum_{i_2 j_2} V_{i_1 j_1 i_2 j_2}^{cc} p_{j_2 i_2} \quad (36)$$

of the external field U . (The explicit form of the renormalization terms considered in this chapter accounts for the Fock contributions only, i.e. no Hartree terms. The general structure of Hartree-Fock contributions, relevant for the case of a strongly non-homogeneous system, is discussed in chapter 6.)

We stress that the Hartree-Fock approximation, which consists in factorizing average values of four-point operators into products of two density

matrices, is independent from the quantum-mechanical picture. This is a general property: any mean-field approximation gives the same result in different representations. The reason is that the mean-field operation commutes with any unitary transformation connecting different basis states. It is then clear that the above kinetic equations are valid in any quantum-mechanical representation.

All the contributions to the system dynamics discussed so far describe a fully coherent dynamics, i.e. no scattering processes. In order to treat incoherent phenomena, e.g. energy relaxation and dephasing, one has to go one step further in the perturbation expansion taking into account also second-order contributions (in the perturbation Hamiltonian \mathbf{H}_{mb}). The derivation of these higher-order contributions, discussed in chapter 6, will not be repeated here. Again, as for the first-order contributions (Hartree-Fock terms), in order to obtain a closed set of equations (with respect to our set of kinetic variables (25-26)) additional approximations are needed, namely the mean-field and the Markov approximation. As for the Hartree-Fock case, the mean-field approximation allows to write the various higher-order density matrices as products of single-particle ones. The Markov approximation allows to eliminate the additional higher-order kinetic variables, e.g. phonon-assisted density matrices, providing a closed set of equations still local in time, i.e. no memory effects [35, 36, 37, 38]. This last approximation is not performed in the quantum-kinetic theory discussed in chapter 6 where, in addition to our single-particle variables, one considers two-particle and phonon-assisted density matrices [34, 38].

While the mean-field approximation is representation-independent, this is unfortunately not the case for the Markov limit. This clearly implies that the validity of the Markov approximation is strictly related to the quantum-mechanical representation considered. We will come back to this point in the following section where the two different pictures used for the study of the carrier dynamics in superlattices are discussed.

The above kinetic description, based on intra- and interband density matrices, allows us to evaluate any single-particle quantity. In particular, for the analysis of semiconductor superlattices two physical quantities play a central role: the intra- and interband total (or macroscopic) polarizations:

$$P^{e/h}(t) = \sum_{ll'} M_{ll'}^{e/h} f_{l'l}^{e/h}(t) , \quad P^{eh} = \sum_{ij} \mu_{ij}^{eh} p_{ji}(t) , \quad (37)$$

where $M^{e/h}$ and μ^{eh} denote, respectively, the intra- and interband dipole matrix elements in our ϕ -representation. The time derivative of the intra-band polarization $P^{e/h}$ describes the radiation field induced by the Bloch-oscillation dynamics (which for a superlattice structure is in the TeraHertz range) while the Fourier transform of the interband (or optical) polarization P^{eh} provides the optical-absorption spectrum.

4 Two equivalent pictures

In this section we will apply the theoretical approach presented so far to the case of a semiconductor superlattice in the presence of an uniform (space-independent) electric field. The non-interacting carriers within the superlattice crystal will then be described by the Hamiltonian \mathbf{H}_c^o in Eq. (10), where now the electrodynamic potentials \mathbf{A}_2 and φ_2 (in the following simply denoted with \mathbf{A} and φ) correspond to a homogeneous electric field $\mathbf{E}_2(\mathbf{r}, t) = \mathbf{F}(t)$.

As pointed out in Sect. 3.1, the natural quantum-mechanical representation is given by the eigenstates of this Hamiltonian:

$$\left[\frac{(-i\hbar\nabla_{\mathbf{r}} - \frac{e}{c}\mathbf{A}(\mathbf{r}, t))^2}{2m_o} + e\varphi(\mathbf{r}, t) + V^l(\mathbf{r}) \right] \phi_n(\mathbf{r}) = \epsilon_n \phi_n(\mathbf{r}) . \quad (38)$$

However, due to the gauge freedom discussed in Sect. 3.1, there is an infinite number of possible combinations of \mathbf{A} and φ —and therefore of possible Hamiltonians— which describe the same homogeneous electric field $\mathbf{F}(t)$. In particular, one can identify two independent choices: the vector-potential gauge

$$\mathbf{A}(\mathbf{r}, t) = -c \int_{t_o}^t \mathbf{F}(t') dt' , \quad \varphi(\mathbf{r}, t) = 0 \quad (39)$$

and the scalar-potential gauge

$$\mathbf{A}(\mathbf{r}, t) = 0 , \quad \varphi(\mathbf{r}, t) = -\mathbf{F}(t) \cdot \mathbf{r} \quad (40)$$

(previously employed for the description of the laser photoexcitation in Eq. (7)).

As we will see, the two independent choices correspond, respectively, to the well known Bloch-oscillation and Wannier-Stark pictures. They simply reflect two equivalent quantum-mechanical representations and, therefore, any physical phenomenon can be described in both pictures.

4.1 The Bloch-oscillation picture

The vector-potential approach presented in this section, originally proposed by Kittel [8], is discussed in Ref. [9].

Within the vector-potential gauge (39), the above eigenvalue equation (38) reduces to:

$$\left[\frac{(-i\hbar\nabla_{\mathbf{r}} - \frac{e}{c}\mathbf{A}(t))^2}{2m_o} + V^l(\mathbf{r}) \right] \phi_n(\mathbf{r}) = \epsilon_n \phi_n(\mathbf{r}) . \quad (41)$$

In this gauge the vector potential is space-independent but, even for the case of a static field ($\mathbf{F}(t) = \mathbf{F}_o$), it is always time-dependent. Therefore, the above Hamiltonian (together with its eigenvalues and eigenfunctions)

will be time dependent as well. However, for any time t we can consider its “instantaneous” eigenstates $\phi_n(\mathbf{r}, t)$. They can be easily evaluated by means of the following transformation:

$$\phi_n(\mathbf{r}, t) = \phi_n^\circ(\mathbf{r}, t) e^{\frac{i\epsilon}{\hbar c} \chi(\mathbf{r}, t)} \quad (42)$$

with

$$\chi(\mathbf{r}, t) = \mathbf{A}(t) \cdot \mathbf{r} . \quad (43)$$

By applying this transformation to the eigenvalue problem in Eq. (41), we obtain [9]:

$$\left[-\frac{\hbar^2 \nabla_{\mathbf{r}}^2}{2m_o} + V^l(\mathbf{r}) \right] \phi_n^\circ(\mathbf{r}) = \epsilon_n \phi_n^\circ(\mathbf{r}) , \quad (44)$$

i.e. the wavefunctions $\phi_n^\circ(\mathbf{r})$ are just the Bloch states $\phi_{\mathbf{k}\nu}^\circ(\mathbf{r})$ of our semiconductor, and the energy spectrum ϵ_n coincides with the carrier band structure $\epsilon_{\mathbf{k}\nu}$. Therefore, from Eq. (42) the desired eigenfunctions result to be of the form:

$$\phi_{\mathbf{k}\nu}(\mathbf{r}, t) = \phi_{\mathbf{k}\nu}^\circ(\mathbf{r}, t) e^{\frac{i\epsilon}{\hbar c} \mathbf{A}(t) \cdot \mathbf{r}} . \quad (45)$$

Apart from a phase-factor, they coincide with the conventional Bloch states of the crystal. The reason can be understood as follows: Also in the presence of the electric field \mathbf{F} , the Hamiltonian in Eq. (41) is still invariant under a lattice translation corresponding to the crystal potential V^l . Thus, the crystal momentum $\hbar\mathbf{k}$ is still a “good” quantum number and the band dispersion remains the same: $\epsilon = \epsilon_{\mathbf{k}\nu}$. Therefore, at each time t our time-dependent eigenstates seem to coincide (a part from the phase-factor) with the Bloch states of the crystal and, at a first glance, it is not clear which is the role played by the applied field.

In order to answer this question, let us consider again the general form of our eigenstates in Eq. (45). At the initial time t_o the vector potential \mathbf{A} is equal to zero and, therefore, the two basis sets coincide: $\phi_{\mathbf{k}_o\nu}(\mathbf{r}, t_o) = \phi_{\mathbf{k}\nu}^\circ(\mathbf{r})$. (Here, \mathbf{k}_o and \mathbf{k} denote the carrier wavevectors at time t_o and t , respectively. They are, in principle, independent quantities, since they correspond to two different eigenvalue problems.) In other words, the Bloch states $\phi_{\mathbf{k}\nu}^\circ$ can be also regarded as the states $\phi_{\mathbf{k}_o\nu}$ at the initial time t_o and vice versa. This allows us to rewrite Eq. (45) as

$$\phi_{\mathbf{k}\nu}(\mathbf{r}, t) = \phi_{\mathbf{k}_o\nu}(\mathbf{r}, t_o) e^{\frac{i\epsilon}{\hbar c} \mathbf{A}(t) \cdot \mathbf{r}} \quad (46)$$

or equivalently

$$\phi_{\mathbf{k}\nu}^\circ(\mathbf{r}) = \phi_{\mathbf{k}_o\nu}^\circ(\mathbf{r}) e^{-\frac{i\epsilon}{\hbar c} \mathbf{A}(t) \cdot \mathbf{r}} . \quad (47)$$

Moreover, in view of the translational symmetry of the crystal, at each time t the Bloch states ϕ° should obey the Bloch theorem [8]:

$$\phi_{\mathbf{k}\nu}^\circ(\mathbf{r} + \mathbf{a}) = \phi_{\mathbf{k}\nu}^\circ(\mathbf{r}) e^{i\mathbf{k} \cdot \mathbf{a}} , \quad (48)$$

where \mathbf{a} denotes any periodicity vector of the crystal. If we now apply the

Bloch theorem to both sides of Eq. (47), i.e. at time t and t_0 , we finally obtain:

$$\mathbf{k} = \mathbf{k}_0 - \frac{e}{\hbar c} \mathbf{A}(t) . \quad (49)$$

This result is quite important: the symmetry properties of the Hamiltonian require a precise relationship between the (formally independent) wavevectors \mathbf{k}_0 and \mathbf{k} . More specifically, the carrier wavevector results to be a function of time ($\mathbf{k} = \mathbf{k}(t)$), i.e. the instantaneous sets of basis states $\{\phi_{\mathbf{k}(t)\nu}(\mathbf{r}, t)\}$ (corresponding to different times t) are mutually connected through a continuous time evolution of the wavevector \mathbf{k} . We can then answer the previous question saying that within the vector-potential gauge the application of a homogeneous field $\mathbf{F}(t)$ induces a simple “drift” in \mathbf{k} -space of the crystal Bloch states, which are therefore not “distorted” by the presence of the field.

From a physical point of view, the above equation describes the continuous time evolution of a carrier in \mathbf{k} -space induced by the applied electric field. In particular, taking into account the explicit form of the vector potential \mathbf{A} given in Eq. (39), we have

$$\mathbf{k}(t) = \mathbf{k}_0 + \frac{e}{\hbar} \int_{t_0}^t \mathbf{F}(t') dt' , \quad (50)$$

from which the acceleration theorem in Eq. (1) is recovered:

$$\dot{\mathbf{k}}(t) = \frac{e}{\hbar} \mathbf{F}(t) . \quad (51)$$

As pointed out in the introduction, this is usually regarded as a “semiclassical” result, i.e. as obtained by applying to a Bloch electron the laws of classical mechanics. However, the above analysis shows that this is a rigorous quantum-mechanical result: the quantum evolution of a carrier within a given band ν under the action of a homogeneous electric field is rigorously described by the acceleration theorem.

We want to stress once again that within the vector-potential gauge discussed so far the acceleration theorem is just a result of the symmetry properties of the crystal and the time-dependent eigenstates in Eq. (45) describe the quantum analogue of the “semiclassical motion” of a carrier in \mathbf{k} -space (see Fig. 1).

Let us now consider the case of a static field, i.e. $\mathbf{F}(t) = \mathbf{F}_0$, applied parallel to a symmetry axis of the crystal. In this case, the corresponding vector potential entering Eq. (49) is a linear function of time, which induces a uniform drift of the carriers in \mathbf{k} -space along the field direction:

$$\mathbf{k}(t) = \mathbf{k}_0 + \dot{\mathbf{k}}(t - t_0) = \frac{e\mathbf{F}_0}{\hbar}(t - t_0) . \quad (52)$$

Since the carrier energy —given by the eigenvalue in Eq. (41)— coincides

with the crystal band structure $\epsilon_{\mathbf{k}\nu}$, its time evolution is:

$$\epsilon_{\nu}(t) = \epsilon_{\nu}(\mathbf{k}(t)) = \epsilon_{\nu}\left(\mathbf{k}_o + \dot{\mathbf{k}}(t - t_o)\right) . \quad (53)$$

Due to the periodic nature of the band structure as a function of \mathbf{k} , i.e. $\epsilon_{\nu}(\mathbf{k}) = \epsilon_{\nu}(\mathbf{k} + \mathbf{G})$ (\mathbf{G} being a reciprocal-lattice vector), the carrier will execute a periodic motion in time with a period

$$\tau_B = \frac{h}{eF_o d} , \quad (54)$$

where d is the lattice periodicity (in real space) along the field direction. This coincides with the Bloch period previously introduced (see Sect. 1). It corresponds to the time needed for the electron to travel from any point k to the energetically equivalent point $k + \frac{2\pi}{d}$.

These periodic oscillations of the carrier over the crystal band structure (see Fig. 1) are known as Bloch oscillations. As pointed out in Sect. 1, they were first introduced by Bloch [1] on the basis of semiclassical arguments. However, as for the case of the acceleration theorem discussed above, this is a rigorous quantum-mechanical result of the vector-potential picture discussed so far. Such a clear physical interpretation of the quantum-mechanical theory in terms of a semiclassical picture is hard to obtain within the scalar-potential gauge presented in the following section.

Both the acceleration theorem (51) and the Bloch-oscillation dynamics previously discussed are induced by the noninteracting-carrier Hamiltonian in Eq. (41) through its time-dependent eigenstates $\phi_{\mathbf{k}(t)\nu}$. Therefore, the Bloch-oscillation dynamics considered so far does not account for many-body effects (carrier-carrier and carrier-phonon interactions) as well as for the effects induced by the time variation of our basis states. For a more “realistic” description of the carrier dynamics within our vector-potential picture we are then forced to employ the general kinetic theory presented in Sect. 3.2.

As discussed in chapter 6, for the case of a homogeneous semiconductor crystal the only relevant terms of the single-particle density matrix in our $\mathbf{k}\nu$ representation are those diagonal in \mathbf{k} . This property, which is due again to the translational symmetry of the Hamiltonian, reduces the set of kinetic variables in Eqs. (25-26) to the intraband density-matrix elements

$$f_{\mathbf{k},\alpha\alpha'}^e = \left\langle c_{\mathbf{k}\alpha}^{\dagger} c_{\mathbf{k}\alpha'} \right\rangle , \quad f_{-\mathbf{k},\beta\beta'}^h = \left\langle d_{-\mathbf{k}\beta}^{\dagger} d_{-\mathbf{k}\beta'} \right\rangle \quad (55)$$

plus the interband density-matrix elements

$$p_{\mathbf{k},\beta\alpha} = \left\langle d_{-\mathbf{k}\beta} c_{\mathbf{k}\alpha} \right\rangle . \quad (56)$$

Here, the standard electron-hole picture introduced in Sect. 3.1 has been applied to our set of time-dependent eigenstates $\phi_{\mathbf{k}(t)\nu}$: the band index ν (which refers to both conduction and valence states) is replaced by two

separate band indices α and β for electrons and holes, respectively, while, due to the charge-conjugation symmetry, the hole states are still labeled in terms of the corresponding valence-electron states, i.e. $\mathbf{k}^h\beta \equiv -\mathbf{k}^e\beta$.

Let us now discuss the explicit form of the kinetic equations (31) in our vector-potential picture:

$$\begin{aligned}\frac{d}{dt}f_{\mathbf{k},\alpha_1\alpha_2}^e &= \frac{d}{dt}f_{\mathbf{k},\alpha_1\alpha_2}^e \Big|_{\mathbf{H}} + \frac{d}{dt}f_{\mathbf{k},\alpha_1\alpha_2}^e \Big|_{\phi} \\ \frac{d}{dt}f_{-\mathbf{k},\beta_1\beta_2}^h &= \frac{d}{dt}f_{-\mathbf{k},\beta_1\beta_2}^h \Big|_{\mathbf{H}} + \frac{d}{dt}f_{-\mathbf{k},\beta_1\beta_2}^h \Big|_{\phi} \\ \frac{d}{dt}p_{\mathbf{k},\beta_1\alpha_1} &= \frac{d}{dt}p_{\mathbf{k},\beta_1\alpha_1} \Big|_{\mathbf{H}} + \frac{d}{dt}p_{\mathbf{k},\beta_1\alpha_1} \Big|_{\phi}.\end{aligned}\quad (57)$$

Here, the first term is induced by the system Hamiltonian $\mathbf{H} = \mathbf{H}_{sp} + \mathbf{H}_{mb}$ (which does not account for the time variation of the basis states) while the second one is induced by the time evolution of the basis functions ϕ .

The contributions to the carrier dynamics due to the single-particle Hamiltonian \mathbf{H}_{sp} are given in Eq. (34). They consist in a ‘‘free rotation’’ plus a term due to the interaction with the external laser field. For the case of an ultrafast laser excitation, after the initial carrier photogeneration the only non-vanishing contributions in Eq. (34) are such free-rotation terms. If we now consider that in our vector-potential representation the energy matrix ϵ in Eq. (19) is diagonal,

$$\epsilon_{\mathbf{k}l,\mathbf{k}'l'}^{e/h} = \epsilon_{\mathbf{k}l}^{e/h} \delta_{\mathbf{k}\mathbf{k}'} \delta_{ll'}, \quad (58)$$

the single-particle contributions after the initial photoexcitation reduce to:

$$\begin{aligned}\frac{d}{dt}f_{\mathbf{k},\alpha_1\alpha_2}^e \Big|_{sp} &= \frac{1}{i\hbar} [\epsilon_{\mathbf{k}\alpha_2}^e - \epsilon_{\mathbf{k}\alpha_1}^e] f_{\mathbf{k},\alpha_1\alpha_2}^e \\ \frac{d}{dt}f_{-\mathbf{k},\beta_1\beta_2}^h \Big|_{sp} &= \frac{1}{i\hbar} [\epsilon_{-\mathbf{k}\beta_2}^h - \epsilon_{-\mathbf{k}\beta_1}^h] f_{-\mathbf{k},\beta_1\beta_2}^h \\ \frac{d}{dt}p_{\mathbf{k},\beta_1\alpha_1} \Big|_{sp} &= \frac{1}{i\hbar} [\epsilon_{-\mathbf{k}\beta_1}^h + \epsilon_{\mathbf{k}\alpha_1}^e] p_{\mathbf{k},\beta_1\alpha_1}.\end{aligned}\quad (59)$$

As we can see, the above equations describe a set of independent many-level systems, i.e. one for each \mathbf{k} value. In addition, there is no coupling between different kinetic variables. If, in particular, we assume a diagonal initial condition

$$f_{\mathbf{k},ll'}^{e/h} \equiv f_{\mathbf{k},l}^{e/h} \delta_{ll'}, \quad p_{\mathbf{k},ll'} \equiv p_{\mathbf{k},l} \delta_{ll'} \quad (60)$$

(which is well fulfilled for the case of a laser photoexcitation of standard bulk semiconductors as well as superlattice structures), the kinetic equations (59) for the non-zero density-matrix elements, i.e. for the diagonal ones, reduce to:

$$\frac{d}{dt}f_{\pm\mathbf{k},l}^{e/h} = 0, \quad \frac{d}{dt}p_{\mathbf{k},l} = 0, \quad (61)$$

where the \pm sign refers, respectively, to electrons and holes. If we now remember that in our vector-potential representation the wavevector \mathbf{k} is itself a function of time (see Eq. (49)), the above kinetic equations can be rewritten as:

$$\frac{\partial}{\partial t}f_{\pm\mathbf{k},l}^{e/h} \pm \dot{\mathbf{k}} \cdot \nabla_{\mathbf{k}}f_{\pm\mathbf{k},l}^{e/h} = 0, \quad \frac{\partial}{\partial t}p_{\mathbf{k},l} + \dot{\mathbf{k}} \cdot \nabla_{\mathbf{k}}p_{\mathbf{k},l} = 0. \quad (62)$$

For both distribution functions f and interband polarizations p we obtain a simple drift equation whose general solution is of the form:

$$y(\mathbf{k}(t), t) = y(\mathbf{k}_o, t_o), \quad (63)$$

i.e. the function at time t is obtained through a rigid shift $\Delta\mathbf{k} = \mathbf{k} - \mathbf{k}_o$ of the function at the initial time t_o . Such drift in \mathbf{k} -space, induced by the external field \mathbf{F} , is again described by the acceleration theorem in Eq. (51). Therefore, as expected, the carrier dynamics described by the above kinetic equations (which accounts for the single-particle Hamiltonian only) is fully equivalent to the Bloch-oscillation dynamics discussed above. However, such relatively simple picture of the carrier motion does not account for the time-dependence of our basis states as well as for many-body effects, e.g. carrier-carrier and carrier-phonon interactions.

The contributions to the carrier dynamics induced by the time variation of the basis states are given in Eq. (32). In our vector-potential representation (45) the explicit form of the matrix elements $Z_{ll'}^{e/h}$ introduced in Eq. (30) is

$$Z_{\mathbf{k}l,\mathbf{k}'l'}^{e/h} = Z_{\mathbf{k},ll'}^{e/h} \delta_{\mathbf{k}\mathbf{k}'} \quad (64)$$

with

$$Z_{\mathbf{k},ll'}^{e/h} = \pm e (\delta_{ll'} - 1) \int d\mathbf{r} \phi_{\mathbf{k}l}^{e/h*} [\mathbf{F}(t) \cdot \mathbf{r}] \phi_{\mathbf{k}l'}^{e/h}. \quad (65)$$

They result to be strictly related to the matrix elements of the scalar potential in Eq. (40), as we will discuss in the following section. The $\mathbf{k}l \rightarrow \mathbf{k}'l'$ transitions induced by the time variation of the basis states are always diagonal in \mathbf{k} ; this reflects the momentum conservation in the carrier-field interaction, i.e. since the momentum \mathbf{q} corresponding to a space-independent field is equal to zero, the initial and final carrier wavevectors coincide. Moreover, there are no intraband ($l = l'$) transitions, which confirms that the action of the field within a given band is fully described by the drift terms in Eq. (62).

If we now rewrite Eq. (32) in our vector-potential representation taking

into account the explicit form of the above matrix elements, we finally obtain:

$$\begin{aligned}
\left. \frac{d}{dt} f_{\mathbf{k},\alpha_1\alpha_2}^e \right|_{\phi} &= \frac{1}{i\hbar} \sum_{\alpha_3\alpha_4} [Z_{\mathbf{k},\alpha_2\alpha_4}^e \delta_{\alpha_1\alpha_3} - Z_{\mathbf{k},\alpha_3\alpha_1}^e \delta_{\alpha_2\alpha_4}] f_{\mathbf{k},\alpha_3\alpha_4}^e \\
\left. \frac{d}{dt} f_{-\mathbf{k},\beta_1\beta_2}^h \right|_{\phi} &= \frac{1}{i\hbar} \sum_{\beta_3\beta_4} [Z_{-\mathbf{k},\beta_2\beta_4}^h \delta_{\beta_1\beta_3} - Z_{-\mathbf{k},\beta_3\beta_1}^h \delta_{\beta_2\beta_4}] f_{-\mathbf{k},\beta_3\beta_4}^h \\
\left. \frac{d}{dt} p_{\mathbf{k},\beta_1\alpha_1} \right|_{\phi} &= \frac{1}{i\hbar} \sum_{\alpha_2\beta_2} [Z_{-\mathbf{k},\beta_1\beta_2}^h \delta_{\alpha_1\alpha_2} + Z_{\mathbf{k}\alpha_1\alpha_2}^e \delta_{\beta_1\beta_2}] p_{\mathbf{k},\beta_2\alpha_2}. \quad (66)
\end{aligned}$$

From the above kinetic equations we clearly see that the time variation of our basis states ϕ induces “vertical” (i.e. $\mathbf{k} = \mathbf{k}'$) transitions between different bands. Such interband coupling is the well known Zener tunneling [2]. This effect is usually described as an interband transition induced by the scalar potential $-\mathbf{F} \cdot \mathbf{r}$, which is also evident from the explicit form of the Zener matrix elements in Eq. (65). However, within our vector-potential picture the Zener tunneling originates from the time variation of our accelerated Bloch states in Eq. (45).

As discussed in Ref. [9], for the case of bulk semiconductors this interband coupling results to be very limited even for the case of high applied fields. Therefore, the Bloch-oscillation scenario of the semiclassical theory (see Fig. 1) is practically unmodified by Zener tunneling. For the case of interest, i.e. that of semiconductor superlattices, interminiband Zener tunneling is expected to play a significant role in the high-field regime. However, for relatively low fields (up to 10^4V/cm) the effect is again negligible and the Bloch-oscillation regime is fully recovered. In this case, the time-scale of Zener-tunneling processes is much longer than the Bloch-oscillation period τ_B . Therefore, the effect due to the time variation of our basis states is negligible, i.e. the time variation can be regarded as an “adiabatic transformation”.

Let us finally consider the role played by many-body effects, i.e. carrier-carrier and carrier-phonon interactions. As discussed in Sect. 3.2 as well as in chapter 6, these many-body effects can be divided into coherent and incoherent contributions. With coherent contributions we refer to first-order terms in the many-body Hamiltonian \mathbf{H}_{mb} . Since we neglect coherent-phonon states, the only non-zero contributions originate from carrier-carrier interaction. The explicit form of these Hartree-Fock terms in our vector-potential representation is obtained from Eqs. (35-36) by replacing the generic labels i and j with $\mathbf{k}\alpha$ and $-\mathbf{k}\beta$, respectively.

From a physical point of view, these coherent contributions give rise to excitonic and band-renormalization effects, which result in a modification of the single-particle energy spectrum. In our case, these excitonic effects may

lead to modifications of the Bloch-oscillation dynamics, e.g. small variations of the Bloch period. As we will see, within the Wannier-Stark picture such excitonic effects manifest themselves in a modification of the single-particle Wannier-Stark energy levels, which are not equidistantly spaced anymore [39].

Let us now come to the role played by incoherent contributions, i.e. second-order contributions in the many-body Hamiltonian. As pointed out in Sect. 3.2, these terms are usually treated within the usual Markov approximation. The resulting contributions describe, in general, second-order transitions connecting all possible kinetic variables, i.e. all possible density-matrix elements. The transitions connecting diagonal density-matrix elements, i.e. distribution functions, can be easily described in terms of stochastic scattering processes, i.e. due to the scattering with a partner carrier or with a phonon, the electron may undergo a transition from an initial state $\mathbf{k}\nu$ to a final state $\mathbf{k}'\nu'$. On the contrary, for the transitions involving non-diagonal terms the second-order coupling is not positive-definite, i.e. it is not a rate, and the intuitive scattering picture cannot be employed.

It is not in the spirit of this chapter to derive and discuss the explicit form of the second-order carrier-carrier and carrier-phonon contributions. From a physical point of view, both carrier-carrier and carrier-phonon scattering processes give rise to energy relaxation and dephasing. It is well known that, due to scattering events, a photogenerated carrier distribution will relax both energy and momentum and, in addition, it will lose its internal degree of coherence, which corresponds to a decay of the interband polarizations. This stochastic dynamics may strongly influence the deterministic Bloch-oscillation regime discussed so far [40, 41, 42].

As we will see from some simulated experiments reported in Sect. 5, the role played by carrier-carrier and carrier-phonon scattering strongly depends on the physical conditions considered, e.g. carrier density, excitation energy, and lattice temperature. When the scattering rate corresponding to the dominant interaction mechanism is much larger than the Bloch oscillation frequency $\omega_B = \frac{2\pi}{\tau_B}$, the Bloch oscillations are not suppressed, i.e. the carriers perform on average several Bloch oscillations between two scattering events. On the contrary, if the scattering rate is larger than the Bloch frequency, the carrier cannot execute a full oscillation without scattering. In this case, the Bloch oscillations are totally suppressed and we deal with a diffusive-transport regime.

As discussed in the introductory part of this chapter, in bulk semiconductors also for very high fields the Bloch-oscillation period is larger than the typical scattering times. On the contrary, in semiconductor superlattices the Bloch period is at least one order of magnitude smaller than in bulk systems and, therefore, comparable or even smaller than the typical scattering times.

This allows us to answer the controversial question: “do Bloch oscillations

really exist?”. The analysis presented in this section shows that, in the absence of scattering events, Bloch oscillations exist and, contrary to the early papers by Rabinovitch and Zak [29], they are not significantly affected by Zener tunneling, both for bulk and superlattices.

On the contrary, due to scattering events, Bloch oscillations are fully suppressed in bulk semiconductors but they still survive in superlattices, as confirmed by several experiments [16, 18, 22, 23, 40].

In the following section we will discuss the so-called Wannier-Stark picture. Contrary to the vector-potential approach discussed so far, this will correspond to a scalar-potential representation. In particular, we will study the link between the two pictures showing that phenomena which are peculiar of one picture can be equally described within the second one.

4.2 The Wannier-Stark picture

Within the scalar-potential gauge (40), the eigenvalue equation (38) reduces to:

$$H_c^\circ \phi(\mathbf{r}) = \left[-\frac{\hbar^2 \nabla_{\mathbf{r}}^2}{2m_o} + V^l(\mathbf{r}) - e\mathbf{F} \cdot \mathbf{r} \right] \phi(\mathbf{r}) = \epsilon \phi(\mathbf{r}) . \quad (67)$$

In this gauge the scalar potential is space dependent but, for the case of a static field considered in this section, it is always time independent.

As originally pointed out by Wannier [6], due to the translational symmetry of the crystal potential $V^l(\mathbf{r}) = V^l(\mathbf{r} + \mathbf{d})$, \mathbf{d} being the primitive lattice vector along the field direction, if $\phi(\mathbf{r})$ is an eigenfunction of the Hamiltonian in Eq. (67) with eigenvalue ϵ , then any $\phi(\mathbf{r} + n\mathbf{d})$ is also an eigenfunction with eigenvalue $\epsilon + n\Delta\epsilon$, where $\Delta\epsilon = eFd$ is the so-called Wannier-Stark splitting. However, as pointed out by Zak [7], for the case of an infinite crystal the scalar potential $-\mathbf{F} \cdot \mathbf{r}$ is not bounded, which implies a continuous energy spectrum. This was the starting point of the long-standing controversy on the existence of Wannier-Stark ladders discussed in Sect. 2.

Today, after three decades, we know that the problem is by itself ill-defined and eigenstates can be defined only asymptotically [10]. In particular, there exist ladders of metastable Wannier-Stark states weakly coupled (through Zener tunneling) to a continuous energy spectrum.

We will now study the explicit form of these Wannier-Stark states. As a starting point, let us write the generic eigenstate ϕ as a superposition of conventional Bloch states $\phi_{\mathbf{k}\nu}^\circ$, i.e. let us move to the so-called crystal-momentum representation (CMR):

$$\phi(\mathbf{r}) = \sum_{\mathbf{k}\nu} s_{\mathbf{k}\nu} \phi_{\mathbf{k}\nu}^\circ(\mathbf{r}) = \sum_{\mathbf{G}\nu} \frac{1}{\Omega} \int^{\Omega} d\mathbf{k} s_{\mathbf{k}+\mathbf{G}\nu} \phi_{\mathbf{k}+\mathbf{G}\nu}^\circ(\mathbf{r}) , \quad (68)$$

where \mathbf{G} is a generic reciprocal-lattice vector while Ω denotes the volume

of the first Brillouin zone. Due to the periodicity of the Bloch states in \mathbf{k} -space ($\phi_{\mathbf{k}+\mathbf{G}\nu}^{\circ} = \phi_{\mathbf{k}\nu}^{\circ}$), we are allowed to limit the above expansion to the first Brillouin zone, which implies to impose the same periodicity on the coefficients $s_{\mathbf{k}\nu}$: $s_{\mathbf{k}+\mathbf{G}\nu} = s_{\mathbf{k}\nu}$. By inserting the above expansion (limited to the first Brillouin zone) in Eq. (67), our eigenvalue problem can be rewritten as:

$$\sum_{\nu'} \frac{1}{\Omega} \int^{\Omega} d\mathbf{k}' H_{\mathbf{k}\nu, \mathbf{k}'\nu'}^{\circ} s_{\mathbf{k}'\nu'} = \epsilon s_{\mathbf{k}\nu} , \quad (69)$$

where

$$H_{\mathbf{k}\nu, \mathbf{k}'\nu'}^{\circ} = \epsilon_{\mathbf{k}\nu} \delta_{\mathbf{k}\nu, \mathbf{k}'\nu'} + H_{\mathbf{k}\nu, \mathbf{k}'\nu'}^{\mathbf{F}} \quad (70)$$

are the matrix elements of the Hamiltonian H_c° in the CMR. The first term corresponds to the perfect (field-free) crystal while the second one describes the scalar-potential term:

$$H_{\mathbf{k}\nu, \mathbf{k}'\nu'}^{\mathbf{F}} = -e \int d\mathbf{r} \phi_{\mathbf{k}\nu}^{\circ*} [\mathbf{F} \cdot \mathbf{r}] \phi_{\mathbf{k}'\nu'}^{\circ} . \quad (71)$$

Following the approach discussed in Ref. [34], the above scalar-potential matrix elements can be divided into intraband ($\nu = \nu'$) and interband ($\nu \neq \nu'$) terms: The intraband terms can always be written as a drift operator [34, 43, 44]

$$\frac{1}{\Omega_{\parallel}} \int^{\Omega_{\parallel}} dk'_{\parallel} H_{\mathbf{k}\nu, \mathbf{k}'\nu}^{\mathbf{F}} = -ieF \delta_{k_{\perp} k'_{\perp}} \frac{\partial}{\partial k_{\parallel}} \quad (72)$$

(k_{\parallel} and k_{\perp} being, respectively, the components of the wavevector \mathbf{k} parallel and perpendicular to the field) while the non-diagonal terms coincide with the Zener-tunneling matrix elements Z in Eq. (64). As already pointed out in Sect. 4.1, the Zener tunneling, which in the vector-potential representation is induced by the time variation of the basis states, corresponds to interband transitions induced by the scalar potential in Eq. (40).

For moderate values of the applied field, Zener tunneling to other bands can be neglected and, by inserting Eqs. (70,72) into Eq. (69), our eigenvalue equation reduces to

$$\frac{\partial}{\partial k_{\parallel}} s_{\mathbf{k}\nu} = -\frac{i}{eF} (\epsilon_{\mathbf{k}\nu} - \epsilon) s_{\mathbf{k}\nu} , \quad (73)$$

whose solution is given by:

$$s_{\mathbf{k}\nu} = \delta_{k_{\perp} \tilde{k}_{\perp}} e^{-\frac{i}{eF} \int_0^{k_{\parallel}} (\epsilon_{\kappa'_{\parallel} \tilde{k}_{\perp} \nu} - \epsilon) dk'_{\parallel}} . \quad (74)$$

As expected, the coefficients are diagonal with respect to k_{\perp} , i.e. the linear combination in Eq. (68) will only involve Bloch states with the same perpendicular component k_{\perp} . This reflects the translational symmetry of the Hamiltonian with respect to the plane perpendicular to the field. Moreover,

the periodicity condition $s_{\mathbf{k}+\mathbf{G}\nu} = s_{\mathbf{k}\nu}$ (applied along the field direction) requires that

$$\frac{1}{eF} \int_{-\frac{\pi}{d}}^{+\frac{\pi}{d}} (\epsilon_{k_{\parallel}k_{\perp}\nu} - \epsilon) dk_{\parallel} = 2\pi n \quad (75)$$

which, in turn, tells us that the only allowed energy values are

$$\epsilon = \epsilon^{k_{\perp}n\nu} = \epsilon^{k_{\perp}0\nu} + n eFd \quad (76)$$

with

$$\epsilon^{k_{\perp}0\nu} = \frac{d}{2\pi} \int_{-\frac{\pi}{d}}^{+\frac{\pi}{d}} \epsilon_{k_{\parallel}k_{\perp}\nu} dk_{\parallel} . \quad (77)$$

What we obtain is the Wannier-Stark ladder mentioned above, whose central ($n = 0$) value is given by the average of the band along the field direction (for a given k_{\perp}).

Let us now discuss the corresponding wavefunctions. By inserting in the expansion (68) the explicit form of the coefficients $s_{\mathbf{k}\nu}$ given in Eq. (74) we have:

$$\phi^{k_{\perp}n\nu}(\mathbf{r}) = \frac{d}{2\pi} \int_{-\frac{\pi}{d}}^{+\frac{\pi}{d}} dk_{\parallel} e^{-\frac{i}{eF} \int_0^{k_{\parallel}} (\epsilon_{k'_{\parallel}k_{\perp}\nu} - \epsilon^{k_{\perp}n\nu}) dk'_{\parallel}} \phi_{k_{\parallel}k_{\perp}\nu}^{\circ}(\mathbf{r}) . \quad (78)$$

They are the so-called Wannier-Stark states shown in Fig. 2. For each band ν (and for any given k_{\perp}), we have a set of energetically equidistant states $\phi^{k_{\perp}n\nu}$, obtained from the central ($n = 0$) state $\phi^{k_{\perp}0\nu}$ through the spatial translation $\mathbf{r} \rightarrow \mathbf{r} + n\mathbf{d}$ discussed above. As schematically depicted in Fig. 2, each state is localized around one of the atomic cells of the superlattice and the degree of localization depends on the strength of the applied field F . More precisely, when the Wannier-Stark energy eFd is much smaller than the superlattice miniband width, the wavefunction $\phi^{k_{\perp}n\nu}$ are weakly localized, they extend over several elementary cells. On the contrary, when eFd is comparable or larger than the miniband width, the localization increases and the function results to be significantly different from zero only in one cell. Since the miniband width of the holes is smaller than that of the electrons, the hole states exhibit a stronger Wannier-Stark localization (see Fig. 2).

Due to the neglect of interband Zener tunneling, each Wannier-Stark state $\phi^{k_{\perp}n\nu}$ in Eq. (78) is obtained as a linear combination of Bloch states belonging to the same band ν . Moreover, we see that all Bloch states have the same weight in the expansion, i.e. the coefficients are just phase-factors.

The coefficients s introduced so far can be regarded as the matrix elements of a unitary transformation connecting the Bloch to the Wannier-Stark representation. It is then clear that the inverse transformation allows us to write any Bloch state as a linear combination of Wannier-Stark states:

$$\phi_{\mathbf{k}\nu}^{\circ} = \sum_n s_{\mathbf{k}\nu}^{n*} \phi^{k_{\perp}n\nu}(\mathbf{r}) . \quad (79)$$

The Wannier-Stark states in Eq. (78) can now be used as basis states for our kinetic description. The kinetic variables in the Wannier-Stark representation will be formally the same as for the vector-potential picture discussed in Sect. 4.1. They are defined according to Eqs. (55,56) where the three-dimensional wavevector \mathbf{k} is replaced by its perpendicular component k_{\perp} while the band index α/β is replaced by the same band index plus the Wannier-Stark ladder index n .

Provided the above label substitution, the time evolution of the new kinetic variables is again described by Eq. (57). However, within our Wannier-Stark representation the basis states are time-independent and, therefore, the ϕ -contributions in Eq. (57) are equal to zero. Moreover, contrary to the vector-potential case, the energy matrix ϵ in Eq. (19) is not diagonal. The diagonal terms are now given by the Wannier-Stark ladders in Eq. (76) while the non-diagonal terms are once again Zener-tunneling matrix elements between different Wannier-Stark states.

As already pointed out in Sect. 3.2, the coherent contributions entering our kinetic equations are independent from the quantum-mechanical representation considered. This tells us that the Zener-tunneling contributions to the equations of motion in the scalar- and vector-potential representations should coincide. In fact, in spite of their different physical interpretations (in the vector-potential picture they are induced by the time variation of the basis states while in the scalar-potential one they are due to inter-band transitions induced by the field Hamiltonian), their formal structure is exactly the same, as can be seen by comparing Eqs. (32) and (34).

On the contrary, incoherent contributions, i.e. scattering terms derived within Markov approximation, are expected to be representation-dependent. In particular, within the vector-potential picture the scattering terms are usually derived by neglecting the time dependence of the basis states $\phi_{\mathbf{k}(t)\nu}$, which corresponds to neglecting the action of the field, i.e. the time variation of the carrier wavevector $\mathbf{k}(t)$, during the collision. Within the Wannier-Stark picture, the basis states are time-independent and the standard Markov limit automatically accounts for the so-called intracollisional field effect [34, 35, 36]. However, for moderate values of the applied field incoherent contributions evaluated in the scalar- and vector-potential representations coincide.

Before concluding this section, let us try to better understand the physical link between the accelerated Bloch states of the vector-potential picture and the Wannier-Stark states of the scalar-potential representation. Both basis sets have been introduced as eigenstates of two equivalent Hamiltonians, corresponding to the two different electromagnetic gauges (see Eqs. (41) and (67)). However, it is well known [45] that the solutions of the corresponding time-dependent Schrödinger equations coincide (a part from a phase-factor which is physically irrelevant). More specifically, let us

consider the generic time-dependent Schrödinger equation

$$i\hbar \frac{d}{dt} \psi(\mathbf{r}, t) = H(t) \psi(\mathbf{r}, t) \quad (80)$$

together with the corresponding eigenvalue problem

$$H(t) \phi_\lambda(\mathbf{r}, t) = \epsilon_\lambda(t) \phi_\lambda(\mathbf{r}, t) . \quad (81)$$

The generic solution ψ at time t is given by a linear combination of the eigenstates ϕ according to the time evolution induced by the Hamiltonian H :

$$\psi(\mathbf{r}, t) = \sum_\lambda S_\lambda e^{-\frac{i}{\hbar} \int_{t_0}^t \epsilon_\lambda(t') dt'} \phi_\lambda(\mathbf{r}, t) , \quad (82)$$

which, for the case of the vector-potential Hamiltonian (41) and the corresponding eigenstates in Eq. (45) reduces to:

$$\psi(\mathbf{r}, t) = e^{\frac{ie}{\hbar c} \mathbf{A}(t) \cdot \mathbf{r}} \sum_{\mathbf{k}_0 \nu} S_{\mathbf{k}_0 \nu} e^{-\frac{i}{\hbar} \int_{t_0}^t \epsilon_{\mathbf{k}(t') \nu} dt'} \phi_{\mathbf{k}(t) \nu}^\circ(\mathbf{r}) , \quad (83)$$

where $\mathbf{k}_0 = \mathbf{k}(t_0)$ denotes the carrier wavevector at the initial time t_0 . As discussed in Ref. [9], it is always possible to consider the gauge transformation connecting the above vector-potential picture to the scalar-potential one. The generator of this gauge transformation is the function $-\mathbf{A}(t) \cdot \mathbf{r}$, which tells us that, going from the vector- to the scalar-potential picture, the first phase-factor in Eq. (83) cancels exactly with the corresponding phase-factor of the gauge transformation. Thus, the time-dependent wave function (83) in the scalar-potential gauge reduces to:

$$\psi(\mathbf{r}, t) = \sum_{\mathbf{k}_0 \nu} S_{\mathbf{k}_0 \nu} e^{-\frac{i}{\hbar} \int_{t_0}^t \epsilon_{\mathbf{k}(t') \nu} dt'} \phi_{\mathbf{k}(t) \nu}^\circ(\mathbf{r}) . \quad (84)$$

This is a linear combination of the so-called Houston states [3] originally introduced as time-dependent solutions of the scalar-potential Schrödinger equation.

On the other hand, within the Wannier-Stark representation (78), the linear combination in Eq. (82) reduces to:

$$\psi(\mathbf{r}, t) = \sum_{k_\perp n \nu} S^{k_\perp n \nu} e^{-\frac{i}{\hbar} \epsilon^{k_\perp n \nu} (t-t_0)} \phi^{k_\perp n \nu}(\mathbf{r}) . \quad (85)$$

It is then clear that for a given initial condition $\psi(\mathbf{r}, t_0)$ the two last linear combinations must give at any time t the same wavefunction ψ . Let us consider as initial condition a single Wannier-Stark state $\phi^{k_\perp n \nu}$. According to Eq. (85), at time t the function ψ differs from that at time t_0 only by a phase-factor, which implies that this will be a stationary state, i.e. the wavefunction will remain localized around a given cell and $|\psi|^2$ will not change in time. Therefore, it should be possible to choose the coefficients S

entering Eq. (84) in such a way that the corresponding expansion in terms of Houston states will provide the same stationary Wannier-Stark state.

In order to determine the explicit form of the coefficients corresponding to a stationary state, let us rewrite Eq. (84), replacing at each time t the sum over \mathbf{k}_o with an equivalent sum over the instantaneous $\mathbf{k} = \mathbf{k}_o + \dot{\mathbf{k}}(t - t_o)$ (see Eq. (52)):

$$\psi(\mathbf{r}, t) = \sum_{\mathbf{k}\nu} S_{\mathbf{k}-\dot{\mathbf{k}}(t-t_o)\nu} e^{-\frac{i}{\hbar} \int_{t_o}^t \epsilon_{\mathbf{k}(t')\nu} dt'} \phi_{\mathbf{k}\nu}^o(\mathbf{r}). \quad (86)$$

The stationary-state condition corresponds to impose that each individual term entering the above expansion will evolve in time according to the constant Wannier-Stark energy $\epsilon^{k_\perp n\nu}$,

$$S_{\mathbf{k}-\dot{\mathbf{k}}(t-t_o)\nu} e^{-\frac{i}{\hbar} \int_{t_o}^t \epsilon_{\mathbf{k}(t')\nu} dt'} \propto e^{-\frac{i}{\hbar} \epsilon^{k_\perp n\nu} (t-t_o)}, \quad (87)$$

which implies that for each time t

$$S_{\mathbf{k}-\dot{\mathbf{k}}(t-t_o)\nu} \propto e^{\frac{i}{\hbar} \int_{t_o}^t (\epsilon_{\mathbf{k}(t')\nu} - \epsilon^{k_\perp n\nu}) dt'}. \quad (88)$$

The above time integral over t' can be translated into a corresponding integral over $k' = k_\parallel(t')$:

$$e^{\frac{i\epsilon}{F} \int_{k_o}^k (\epsilon_{k'\nu} - \epsilon^{k_\perp n\nu}) dk'} = e^{\frac{i\epsilon}{F} \int_0^k (\epsilon_{k'\nu} - \epsilon^{k_\perp n\nu}) dk'} e^{-\frac{i\epsilon}{F} \int_0^{k_o} (\epsilon_{k'\nu} - \epsilon^{k_\perp n\nu}) dk'}. \quad (89)$$

Since the first phase-factor on the right-hand side is time-independent, we finally obtain:

$$S_{\mathbf{k}_o\nu} \propto e^{-\frac{i\epsilon}{F} \int_0^{k_o} (\epsilon_{k'\nu} - \epsilon^{k_\perp n\nu}) dk'}. \quad (90)$$

As expected, the coefficients S of a stationary state coincide with the coefficients s in Eq. (74). Thus, the linear combinations of accelerated Bloch states corresponding to stationary states are just the Wannier-Stark states introduced in Eq. (78) as eigenstates of the scalar-potential Hamiltonian.

From the above analysis, we see that within a time-dependent approach the scalar- and vector-potential pictures are totally equivalent. According to the initial condition (i.e. depending on the coefficients S), we may have a Bloch-oscillation as well as a Wannier-Stark scenario, or any intermediate regime. If we consider, for example, the case of a laser excitation whose energy spectrum is concentrated around a well defined frequency, this will generate a distribution of photoexcited carriers strongly peaked about a particular k . Each carrier will then be described by a single accelerated Bloch state $\phi_{\mathbf{k}\nu}$ and will execute Bloch oscillations. Thus, the overall motion of this packet in \mathbf{k} -space will resemble the periodic motion of a single electron “prepared” in a Bloch state (see Fig. 3). As we will discuss in the following section, such Bloch-oscillation dynamics can be monitored via four-wave-mixing experiments or THz-signal measurements.

On the contrary, if we perform a linear-absorption measurement using as a light source a laser with uniform spectral distribution, we generate a uniform distribution of photoexcited carriers in \mathbf{k} -space with their proper phase coherence (described by the corresponding interband polarizations). Such distribution is shifted in \mathbf{k} -space but, being almost constant, there is no macroscopic effect. This resembles the situation corresponding to a single electron prepared in a Wannier-Stark state, which is a uniform superposition of Bloch states. This is confirmed by optical-absorption investigations which clearly show the Wannier-Stark energy quantization (see Fig. 7).

5 Some simulated experiments

In this section, we will review recent simulated experiments of the ultrafast carrier dynamics in semiconductor superlattices [41, 42, 46, 47, 48, 49]. They are based on a generalized Monte Carlo solution [50, 51, 52, 53] of the set of kinetic equations (so-called semiconductor Bloch equations) derived in Sect. 3.2. This generalized Monte Carlo approach, successfully applied for the interpretation of ultrafast coherent phenomena in bulk semiconductors [54, 55, 56, 57], is based on a combined solution of our kinetic equations [53]: the coherent contributions are evaluated by means of a direct numerical integration while the incoherent ones are “sampled” by means of a conventional Monte Carlo simulation in the three-dimensional \mathbf{k} -space.

This generalized Monte Carlo method has been recently applied to semiconductor superlattices. As described in Refs. [41, 46], the simulation scheme is based on the Bloch-state representation of the vector-potential picture introduced in Sec. 4.1.

The following superlattice model has been employed: The energy dispersion and the corresponding wavefunctions along the growth direction (k_{\parallel}) are computed within the well known Kronig-Penney model [12], while for the in-plane direction (k_{\perp}) an effective-mass model has been used. Starting from these three-dimensional wavefunctions $\phi_{\mathbf{k}l}^{\circ}$, the various carrier-carrier as well as carrier-phonon matrix elements are numerically computed (see Eqs. (22) and (24)). They are, in general, functions of the various miniband indices and depend separately on k_{\parallel} and k_{\perp} , thus fully reflecting the anisotropic nature of the superlattice structure.

Only coupling to GaAs bulk phonons has been considered. This, of course, is a simplifying approximation which neglects any superlattice effect on the phonon dispersion, such as confinement of optical modes in the wells and in the barriers, and the presence of interface modes [58]. However, while these modifications have important consequences for phonon spectroscopies (like Raman scattering), they are far less decisive for transport phenomena. Indeed, by now it is well known [58, 59] that the total

scattering rates are sufficiently well reproduced if the phonon spectrum is assumed to be bulk-like.

We will start discussing the scattering-induced damping of Bloch oscillations. In particular, we will show that in the low-density limit this damping is mainly determined by optical-phonon scattering [41, 42] while at high densities the main mechanism responsible for the suppression of Bloch oscillations is found to be carrier-carrier scattering [49].

This Bloch-oscillation analysis in the time domain is also confirmed by its counterpart in the frequency domain. As pointed out in Sect. 4, the presence of Bloch oscillations, due to a negligible scattering dynamics, should correspond to Wannier-Stark energy quantization. This is confirmed by the simulated optical-absorption spectra, which clearly show the presence of the field-induced Wannier-Stark ladders introduced in Sect. 4.2 [48].

5.1 Bloch-oscillation analysis

All the simulated experiments presented in this section refer to the superlattice structure considered in Ref. [46]: 111 Å GaAs wells and 17 Å $\text{Al}_{0.3}\text{Ga}_{0.7}\text{As}$ barriers. For such a structure there has been experimental evidence for a THz-emission from Bloch oscillations [23].

In the first set of simulated experiments an initial distribution of photoexcited carriers (electron-hole pairs) is generated by a 100 fs Gaussian laser pulse in resonance with the first-miniband exciton ($\hbar\omega_L \approx 1540$ meV). The strength of the applied electric field is assumed to be 4 kV/cm, which corresponds to a Bloch period $\tau_B = h/eFd$ of about 800 fs.

In the low-density limit (corresponding to a weak laser excitation), incoherent scattering processes do not alter the Bloch-oscillation dynamics. This is due to the following reasons: In agreement with recent experimental [23, 40] and theoretical [41, 42, 46] investigations, for superlattices characterized by a miniband width smaller than the LO-phonon energy —as for the structure considered here— and for laser excitations close to the band gap, at low temperature carrier-phonon scattering is not permitted. Moreover, in this low-density regime carrier-carrier scattering plays no role: Due to the quasi-elastic nature of Coulomb collisions, in the low-density limit the majority of the scattering processes is characterized by a very small momentum transfer; As a consequence, the momentum relaxation along the growth direction is negligible. As a result, on this picosecond time-scale the carrier system exhibits a coherent Bloch-oscillation dynamics, i.e. a negligible scattering-induced dephasing. This can be clearly seen from the time evolution of the carrier distribution as a function of k_{\parallel} (i.e. averaged over k_{\perp}) shown in Fig. 3. During the laser photoexcitation ($t = 0$) the carriers are generated around $k_{\parallel} = 0$, where the transitions are close to resonance with the laser excitation. According to the acceleration theorem (1), the electrons are then shifted in \mathbf{k} -space. When the carriers reach the

border of the first Brillouin zone they are Bragg reflected. After about 800 fs, corresponding to the Bloch period τ_B , the carriers have completed one oscillation in \mathbf{k} -space. As expected, the carriers execute Bloch oscillations without losing the synchronism of their motion by scattering. This is again shown in Fig. 3, where we have plotted: (b) the mean kinetic energy, (c) the current, and (d) its time derivative which is proportional to the emitted far field, i.e. the THz-radiation. (It can be shown that, by neglecting Zener tunneling, the intraband polarization $P^{e/h}$ in Eq. (37) is proportional to the current.) All these three quantities exhibit oscillations characterized by the same Bloch period τ_B . Due to the finite width of the carrier distribution in \mathbf{k} -space (see Fig. 3(a)), the amplitude of the oscillations of the kinetic energy is somewhat smaller than the miniband width. Since for this excitation condition the scattering-induced dephasing is negligible, the oscillations of the current are symmetric around zero, which implies that the time average of the current is equal to zero, i.e. no dissipation.

As already pointed out, this ideal Bloch-oscillation regime is typical of a laser excitation close to gap in the low-density limit. Let us now discuss, still at low densities, the case of a laser photoexcitation high in the band. Figure 4(a) shows the THz-signal as obtained from a set of simulated experiments corresponding to different laser excitations [46]. The different traces correspond to the emitted THz-signal for increasing excitation energies. We clearly notice the presence of Bloch oscillations in all cases. However, the oscillation amplitude and decay (effective damping) is excitation-dependent.

For the case of a laser excitation resonant with the first-miniband exciton considered above (see Fig. 3), we have a strong THz-signal. The amplitude of the signal decreases when the excitation energy is increased. Additionally, there are also some small changes in the phase of the oscillations, which are induced by the electron-LO phonon scattering.

When the laser energy comes into resonance with the transitions between the second electron and hole minibands ($\hbar\omega_L \approx 1625$ meV), the amplitude of the THz-signal increases again. The corresponding THz-transients show an initial part, which is strongly damped and some oscillations for longer times that are much less damped. For a better understanding of these results, we show in Fig. 4(b) the individual THz-signals, originating from the two electron and two heavy-hole minibands for the excitation with $\hbar\omega = 1640$ meV. The Bloch oscillations performed by the electrons within the second miniband are strongly damped due to intra- and interminiband LO-phonon scattering processes [41, 46]. Since the width of this second miniband (45 meV) is somewhat larger than the LO-phonon energy, also intraminiband scattering is possible, whenever the electrons are accelerated into the high-energy region of the miniband. The THz-signal originating from electrons within the first miniband shows an oscillatory behavior with

a small amplitude and a phase which is determined by the time the electrons need to relax down to the bottom of the band.

At the same time, the holes in both minibands exhibit undamped Bloch oscillations, since the minibands are so close in energy that for these excitation conditions no LO-phonon emission can occur. The analysis shows that at early times the THz-signal is mainly determined by the electrons within the second miniband. At later times the observed signal is due to heavy holes and electrons within the first miniband.

The above theoretical analysis closely resembles experimental observations obtained for a superlattice structure very similar to the one modelled here [23]. In these experiments, evidence for THz-emission from Bloch oscillations has been reported. For some excitation conditions these oscillations are associated with resonant excitation of the second miniband. The general behavior of the magnitude of the signals, the oscillations and the damping are close to the results shown in Fig. 4.

Finally, in order to study the density dependence of the Bloch-oscillation damping, let us go back to the case of laser excitations close to gap. Figure 5(a) shows the total (electrons plus holes) THz-radiation as a function of time for three different carrier densities. With increasing carrier density, carrier-carrier scattering becomes more and more important: Due to Coulomb screening, the momentum transfer in a carrier-carrier scattering increases (its typical value being comparable with the screening wavevector). This can be seen in Fig. 5(a), where for increasing carrier densities we realize an increasing damping of the THz-signal. However, also for the highest carrier density considered here we deal with a damping time of the order of 700 fs, which is much larger than the typical dephasing time, i.e. the decay time of the interband polarization, associated with carrier-carrier scattering. The dephasing time is typically investigated by means of four-wave-mixing (FWM) measurements and such multi-pulse experiments can be simulated as well [54, 55]. From a theoretical point of view, a qualitative estimate of the dephasing time is given by the decay time of the “incoherently summed” polarization (ISP) [51]. Figure 5(b) shows such ISP as a function of time for the same three carrier densities of Fig. 5(a). As expected, the decay times are always much smaller than the corresponding damping times of the THz-signals (note the different time-scale in Figs. 5(a) and (b)). This difference can be understood as follows: The fast decay times of Fig. 5(b) reflect the interband dephasing, i.e. the sum of the electron and hole scattering rates. In particular, for the Coulomb interaction this means the sum of electron-electron, electron-hole, and hole-hole scattering. This last contribution is known to dominate and determines the dephasing time-scale. On the other hand, the total THz-radiation in Fig. 5(a) is the sum of the electron and hole contributions. However, due to the small value of the hole miniband width compared with the electron one, the electron contribution will dominate. This is clearly shown in Fig. 6, where the electron (a)

and hole (b) contributions to the THz-radiation are plotted as a function of time (note the different vertical scale). This means that the THz damping in Fig. 5(a) mainly reflects the damping of the electron contribution (see Fig. 6(a)). This decay, in turn, reflects the intraband dephasing of electrons which is due to electron-electron and electron-hole scattering only, i.e. no hole-hole contributions. This clearly explains the different decay times of Fig. 5(a) and Fig. 5(b).

From the above analysis we can conclude that the decay time of the THz-radiation due to carrier-carrier scattering differs considerably from the corresponding dephasing times obtained from a FWM experiment: The first one is a measurement of the intraband dephasing while the second one reflects the interband dephasing.

5.2 Optical-absorption analysis

Let us now discuss the frequency-domain counterpart of the Bloch-oscillation picture considered so far. Similar to what happens in the time domain, for sufficiently high electric fields, i.e. when the Bloch period $\tau_B = h/eFd$ becomes smaller than the dephasing time, the optical spectra of the superlattice are expected to exhibit the frequency-domain counterpart of the Bloch oscillations, i.e. the Wannier-Stark energy quantization discussed in Sect. 4.2. In absence of Coulomb interaction, the Wannier-Stark ladder absorption increases as a function of the photon energy in a step-like fashion. These steps are equidistantly spaced. This spacing, named Wannier-Stark splitting, is proportional to the applied electric field (see Eq. (76)).

The simulated linear-absorption spectra corresponding to a superlattice structure with 95 Å GaAs wells and 15 Å Al_{0.3}Ga_{0.7}As barriers are shown in Fig. 7 [48]. As we can see, the Coulomb interaction gives rise to excitonic peaks in the absorption spectra and introduces couplings between these Wannier-Stark states. Such exciton peaks, which are not equidistantly spaced any more, are often referred to as excitonic Wannier-Stark ladders [39] of the superlattice.

Since for the superlattice structure considered in this simulated experiment [41, 48] the combined miniband width is larger than the typical two- and three-dimensional exciton binding energies, it is possible to investigate the quasi-three dimensional absorption behavior of the delocalized miniband states as well as localization effects induced by the electric field.

For the free-field case, the electron and hole states are completely delocalized in our three-dimensional \mathbf{k} -space. The perturbation induced by the application of a low field (here ≈ 5 kV/cm), couples the states along the field direction and in the spectra the Franz-Keldysh effect, well known from bulk materials, appears: one clearly notices oscillations which increase in amplitude with the field and shift with $F^{2/3}$ from the $n = 0$ and $n = 1$ levels toward the center of the combined miniband.

For increasing field the potential drop over the distance of a few quantum wells eventually exceeds the miniband width and the electronic states become more and more localized. Despite the field-induced energy difference $neFd$, the superlattice potential is equal for quantum wells separated by nd . Therefore, the spectra decouple into a series of peaks corresponding to the excitonic ground states of the individual electron-hole Wannier-Stark levels. Each Wannier-Stark transition contributes to the absorption with a pronounced $1 - s$ exciton peak, plus higher bound exciton and continuum states. The oscillator strength of a transition n is proportional to the overlap between electron and hole wavefunctions centered at quantum wells n' and $n + n'$, respectively. The analysis shows that this oscillator strength is almost exclusively determined by the amplitude of the electron wavefunction in quantum well $n' + n$ since for fields in the Wannier-Stark regime the hole wavefunctions are almost completely localized over one quantum well due to their high effective mass (see Fig. 2). Thus, the oscillator strengths of transitions to higher $|n|$ become smaller with increasing $|n|$ and field.

At high fields (here $> \approx 8$ kV/cm) the separation between the peaks is almost equal to $neFd$. For example, the peak of the $n = 0$ transition which is shifted by the Wannier-Stark exciton binding energy with respect to the center of the combined miniband, demonstrates that the increasing localization also increases the exciton binding energy. This increased excitonic binding reflects the gradual transition from a three- to a two-dimensional behavior.

For intermediate fields there is an interplay between the Wannier-Stark and the Franz-Keldysh effect. Coming from high fields, first the Wannier-Stark peaks are modulated by the Franz-Keldysh oscillations. However, as soon as the separation eFd between neighboring peaks becomes smaller than their spectral widths, the peaks can no longer be resolved individually so that only the Franz-Keldysh structure remains.

Acknowledgments

I wish to thank the colleagues of the Marburg group, S.W. Koch, T. Meier, and P. Thomas, for their essential contributions to the research activity reviewed in this chapter. I am also grateful to A. Di Carlo, M. Gulia, T. Kuhn, E. Molinari, and P.E. Selbmann for stimulating and fruitful discussions.

This work was supported in part by the EC Commission through the Network "ULTRAFASST".

References

- [1] F. Bloch, Z. Phys. **52**, 555 (1928).
- [2] C. Zener, Proc. R. Soc. **145**, 523 (1934).
- [3] W.V. Houston, Phys. Rev. **57**, 184 (1940).
- [4] E.O. Kane, J. Phys. Chem. Solids **12**, 181 (1959)
- [5] P.N. Argyres, Phys. Rev. **126**, 1386 (1962).
- [6] G.H. Wannier, Phys. Rev. **117**, 432 (1960).
- [7] J. Zak, Phys. Rev. Lett. **20**, 1477 (1968).
- [8] C. Kittel, *Quantum Theory of Solids* (Wiley, New York, 1963), p. 190.
- [9] J.B. Krieger and G.J. Iafrate, Phys. Rev. B **33**, 5494 (1986).
- [10] G. Nenciu, Rev. Mod. Phys. **63**, 91 (1991).
- [11] A. Di Carlo, W. Pötz, and P. Vogl, Phys. Rev. B **50**, 8358 (1994). ...
- [12] G. Bastard, *Wave Mechanics of Semiconductor Heterostructures*, Les Editions de Physique (Les Ulis, France, 1989).
- [13] J. Shah, *Ultrafast Spectroscopy of Semiconductors and Semiconductor Nanostructures* (Springer, Berlin, 1996).
- [14] E.E. Mendez, F. Agullo-Rueda, and J.M. Hong, Phys. Rev. Lett. **60**, 2426 (1988).
- [15] P. Voisin, J. Bleuse, C. Bouche, S. Gaillard, C. Alibert, and A. Regreny, Phys. Rev. Lett. **61**, 1639 (1988).
- [16] J. Feldmann, K. Leo, J. Shah, D.A.B. Miller, J.E. Cunningham, T. Meier, G. von Plessen, A. Schulze, P. Thomas, and S. Schmitt-Rink, Phys. Rev. B **46**, 7252 (1992).
- [17] G. von Plessen and P. Thomas, Phys. Rev. B **45**, 9185 (1992).
- [18] K. Leo, P.H. Bolivar, F. Brüggemann, R. Schwedler, Solid State Commun. **84**, 943 (1992).
- [19] P. Leisching, P. Haring Bolivar, W. Beck, Y. Dhaibi, F. Brüggemann, R. Schwedler, H. Kurz, K. Leo, and K. Köhler, Phys. Rev. B **50**, 14389 (1994).
- [20] T. Dekorsy, P. Leisching, K. Kohler, and H. Kurz, Phys. Rev. B **50**, 8106 (1994).
- [21] T. Dekorsy, R. Ott, H. Kurz, and K. Kohler, Phys. Rev. B **51**, 17275 (1995).
- [22] C. Waschke, H.G. Roskos, R. Sscwedler, K. Leo, H. Kurz, and K. Köhler, Phys. Rev. Lett. **70**, 3319 (1993).
- [23] H.G. Roskos, C. Waschke, R. Schwedler, P. Leisching, Y. Dhaibi, H. Kurz, and K. Köhler, Superlattices and Microstructures **15**, 281 (1994).
- [24] G.H. Wannier, Rev. Mod. Phys. **34**, 645 (1962).
- [25] G.H. Wannier and D.R. Fredkin, Phys. Rev. **125**, 1910 (1962).
- [26] G.H. Wannier and J.P. Van Dyke, J. Math. Phys. **9**, 899 (1968).
- [27] G.H. Wannier, Phys. Rev. **181**, 1364 (1969).

- [28] J. Zak, Phys. Rev. **181**, 1366 (1969).
- [29] A. Rabinovitch and J. Zak, Phys. Lett. **40A**, 189 (1972).
- [30] R.W. Koss and L.M. Lambert, Phys. Rev. B **5**, 1479 (1972).
- [31] J. Callaway, Phys. Rev. **130**, 549 (1963).
- [32] J.A. Kash and J.C. Tsang, in *Light Scattering in Solids VI*, edited by M. Cardona and G.Güntherodt, Springer, Berlin (1989), p. 423.
- [33] W. Pötz and P. Kocevar, Phys. Rev. B **28**, 7040 (1983).
- [34] W. Quade, E. Schöll, F. Rossi, and C. Jacoboni, Phys. Rev. B **50**, 7398 (1994).
- [35] R. Brunetti, C. Jacoboni, and F. Rossi, Phys. Rev. B **39**, 10781 (1989).
- [36] F. Rossi, R. Brunetti, and C. Jacoboni, in *Hot Carriers in Semiconductor Nanostructures: Physics and Applications*, edited by J. Shah (Academic Press inc., Boston, 1992), p. 153.
- [37] D.B. Tran Thoai and H. Haug, Phys. Rev. B **47**, 3574 (1993).
- [38] J. Schilp, T. Kuhn, and G. Mahler, Phys. Rev. B **50**, 5435 (1994).
- [39] M.M. Dignam and J.E. Sipe, Phys. Rev. Lett. **64**, 1797 (1990).
- [40] G. von Plessen, T. Meier, J. Feldmann, E.O. Göbel, P. Thomas, K.W. Goossen, J.M. Kuo, and R.F. Kopf, Phys. Rev. B **49**, 14058 (1994).
- [41] F. Rossi, T. Meier, P. Thomas, S.W. Koch, P.E. Selbmann, and E. Molinari, Phys. Rev. B **51**, 16943 (1995).
- [42] F. Rossi, T. Meier, P. Thomas, S.W. Koch, P.E. Selbmann, and E. Molinari, in *Hot Carriers in Semiconductors*, edited by K. Hess, J.-P. Leburton, and U. Ravaioli (Plenum Press, New York, 1996), p. 157.
- [43] T. Meier, G. von Plessen, P. Thomas, and S.W. Koch, Phys. Rev. Lett. **73**, 902 (1994).
- [44] T. Meier, G. von Plessen, P. Thomas, and S.W. Koch, Phys. Rev. B **51**, 14490 (1995).
- [45] L.I. Schiff, *Quantum Mechanics*, 2nd ed. (McGraw-Hill, New York, 1955), p. 275.
- [46] T. Meier, F. Rossi, P. Thomas, and S.W. Koch, Phys. Rev. Lett. **75**, 2558 (1995).
- [47] K.-C. Je, T. Meier, F. Rossi, and S.W. Koch, Appl. Phys. Lett. **67**, 2978 (1995).
- [48] S.W. Koch, T. Meier, T. Stroucken, A. Knorr, J. Hader, F. Rossi, and P. Thomas, in *Microscopic theory of semiconductors: quantum kinetics, confinement and lasers*, edited by S.W. Koch (World Scientific, Singapore, 1995), p. 81.
- [49] F. Rossi, M. Gulia, P.E. Selbmann, E. Molinari, T. Meier, P. Thomas, and S.W. Koch, in *Proc. 23rd ICPS, Berlin, Germany*, edited by M. Scheffler and R. Zimmermann (World Scientific, Singapore, 1996), p. 1775.
- [50] T. Kuhn and F. Rossi, Phys. Rev. Lett. **69**, 977 (1992).
- [51] T. Kuhn and F. Rossi, Phys. Rev. B **46**, 7496 (1992).
- [52] F. Rossi, S. Haas, and T. Kuhn, Phys. Rev. Lett. **72**, 152 (1994).
- [53] S. Haas, F. Rossi, and T. Kuhn, Phys. Rev. B **53**, 12855 (1996).
- [54] A. Lohner, K. Rick, P. Leisching, A. Leitenstorfer, T. Elsaesser, T. Kuhn, F. Rossi, and W. Stolz, Phys. Rev. Lett. **71**, 77 (1993).
- [55] A. Leitenstorfer, A. Lohner, K. Rick, P. Leisching, T. Elsaesser, T. Kuhn, F. Rossi, W. Stolz, and K. Ploog, Phys. Rev. B **49**, 16372 (1994).

- [56] A. Leitenstorfer, A. Lohner, T. Elsaesser, S. Haas, F. Rossi, T. Kuhn, W. Klein, G. Boehm, G. Traenkle, and G. Weimann, *Phys. Rev. Lett.* **73**, 1687 (1994).
- [57] A. Leitenstorfer, T. Elsaesser, F. Rossi, T. Kuhn, W. Klein, G. Boehm, G. Traenkle, and G.W. Weimann, *Phys. Rev. B* **53**, 9876 (1996).
- [58] E. Molinari, in *Confined Electrons and Photons: New Physics and Applications*, edited by E. Burstein and C. Weisbuch (Plenum, New York, 1994).
- [59] H. Rucker, E. Molinari, and P. Lugli, *Phys. Rev. B* **45**, 6747 (1992).

Figure captions

Figure 1 *Schematic illustration of the field-induced coherent motion of an electronic wavepacket initially created at the bottom of a miniband. Here, the width of the miniband exceeds the LO-phonon energy E_{LO} , so that LO-phonon scattering is possible. After Ref. [40].*

Figure 2 *Schematic representation of the transitions from the valence to the conduction band of a superlattice in the Wannier-Stark localization regime. After Ref. [22].*

Figure 3 *Full Bloch-oscillation dynamics corresponding to a laser photoexcitation resonant with the first-miniband exciton. (a) Time evolution of the electron distribution as a function of k_{\parallel} . (b) Average kinetic energy, (c) current, and (d) THz-signal corresponding to the Bloch oscillations in (a).*

Figure 4 *(a) Total THz-signals for eight different spectral positions of the exciting laser pulse: 1540, 1560, \dots , 1680 meV (from bottom to top). (b) Individual THz-signal of the electrons and holes in the different bands for a central spectral position of the laser pulse of 1640 meV. After Ref. [48].*

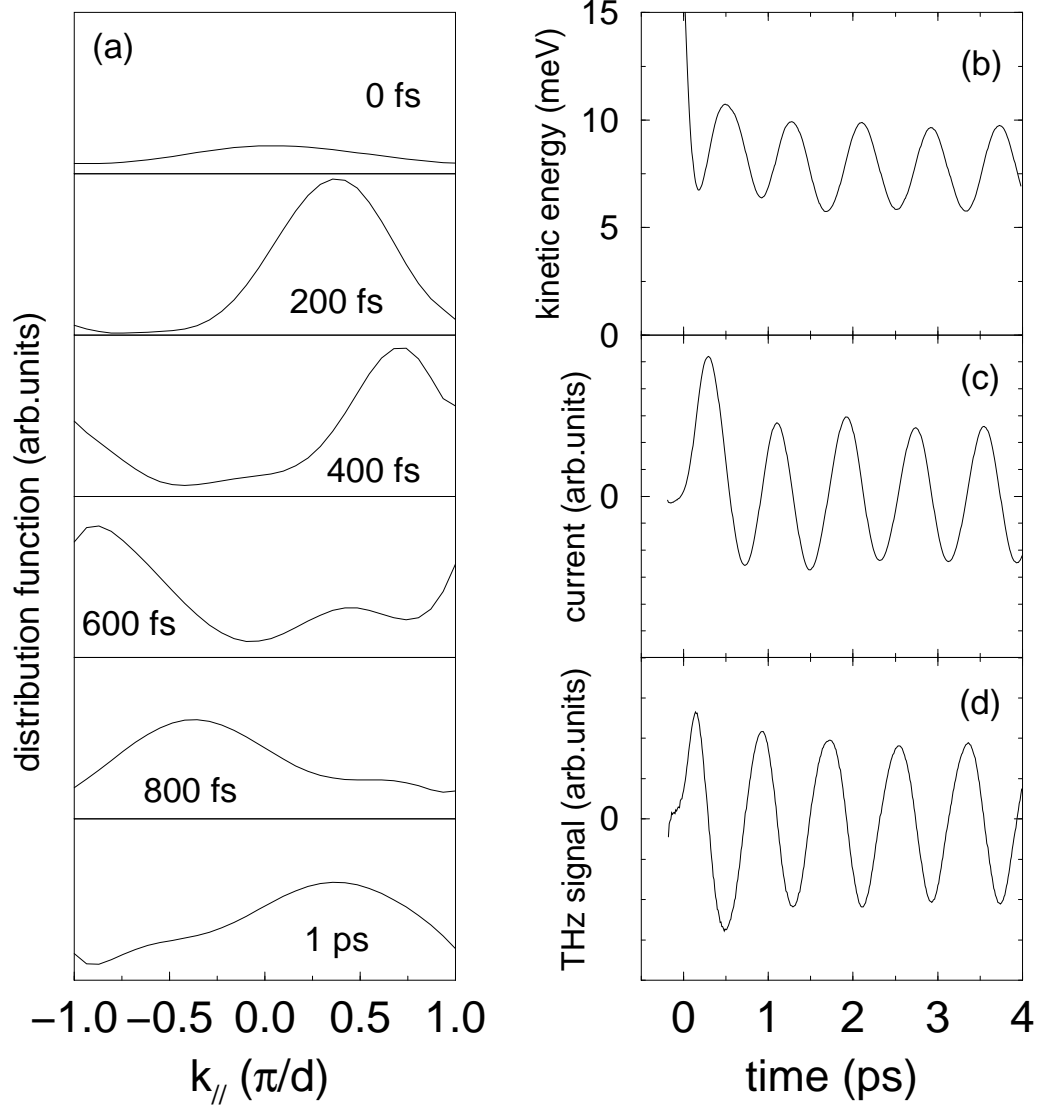
Figure 5 *(a) Total THz-radiation as a function of time; (b) Incoherently-summed polarization as a function of time. After Ref. [49].*

Figure 6 *(a) Electron and (b) hole contributions to the total THz-radiation of Fig. 5(a). After Ref. [49].*

Figure 7 *Absorption spectra for various static applied electric fields for a GaAs/Al_{0.3}Ga_{0.7}As superlattice (well (barrier) width 95 (15) Å). The vertical displacements between any two spectra is proportional to the difference of the corresponding fields. The Wannier-Stark transitions are labeled by numbers, the lower (higher) edge of the combined miniband by E_0 (E_1). After Ref. [48].*

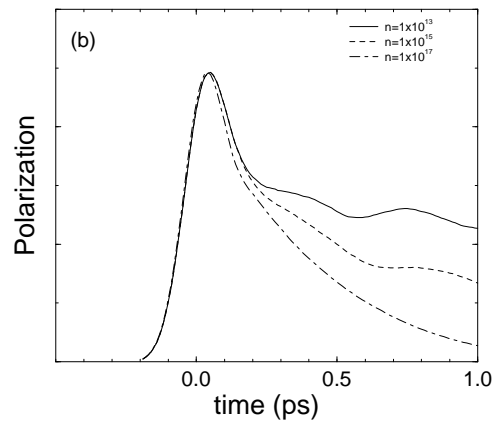
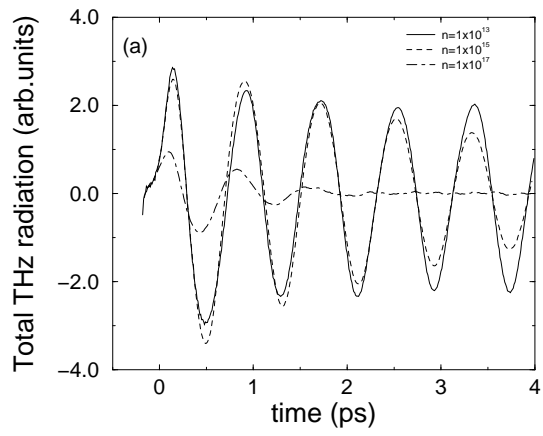
F. Rossi, Fig. 1

F. Rossi, Fig. 2

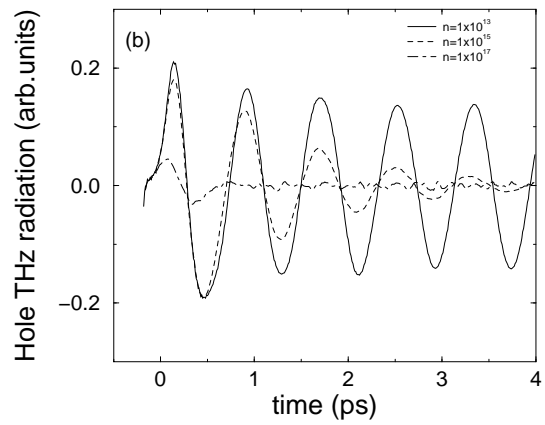
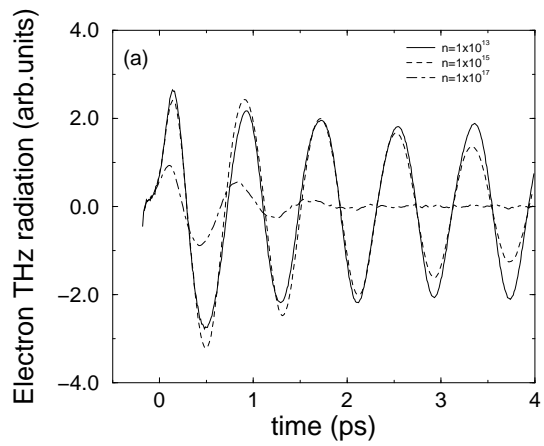


F. Rossi, Fig. 3

F. Rossi, Fig. 4



F. Rossi, Fig. 5



F. Rossi, Fig. 6

F. Rossi, Fig. 7